Article

Not peer-reviewed version

Detecting trends in post-fire forest recovery in Middle Volga from 2000 to 2023

Eldar Kurbanov *, Ludmila Tarasova *, Aydin Yakhyayev, Oleg Vorobev, Siyavush Gozalov, Sergei Lezhnin *, Jinliang Wang, Jinming Sha, Denis Dergunov, Anna Yastrebova

Posted Date: 24 September 2024

doi: 10.20944/preprints202409.1781.v1

Keywords: forest ecosystems; wildfire; burnt area; post-fire forest recovery; Landsat; time-series; GEE; LandTrendr; trend analyses; climatic factors

Article

Detecting Trends in Post-Fire Forest Recovery in Middle Volga from 2000 to 2023

Eldar Kurbanov [1,*], Ludmila Tarasova [1,*], Aydin Yakhyayev [2], Oleg Vorobev [1], Siyavush Gozalov [3], Sergey Lezhnin [1,*], Jinliang Wang [4], Jinming Sha [5], Denis Dergunov [1] and Anna Yastrebova [1]

[1] Center for Sustainable Forest Management and Remote Sensing, Volga State University of Technology, Yoshkar-Ola 424000, Russia
[2] Western Caspian University, School of Advanced Technologies and Natural Sciences, Baku, AZ1001, Azerbaijan; yahyayev-azasu@br.ru
[3] Azerbaijan University of Architecture and Construction, Azerbaijan Republic, AZ-1073.
[4] Faculty of Geography, Yunnan Normal University, Chenggong District, Kunming 650500, China; jlwang@ynnu.edu.cn
[5] School of Geographical Science, Fujian Normal University, Fuzhou 350007, China; jmsha@fjnu.edu.cn
* Correspondence: kurbanovea@volgatech.net, tarasoval@volgatech.net, lejninsa@volgatech.net

Abstract: Increased wildfire activity is the most significant natural disturbance affecting forest ecosystems, with a strong impact on their natural regeneration. This study presents a comprehensive analysis of post-fire forest recovery using Landsat time series data from 2000 to 2023 in the Middle Volga region of the Russian Federation. The analyses utilised the LandTrendr algorithm in Google Earth Engine (GEE) cloud computing platform to examine Normalized Burn Ratio (NBR) spectral metrics and quantify the forest recovery at low, moderate, and high burn severity (BS) levels. To assess the spatio-temporal trends of the recovery, the Mann–Kendall statistical test and Theil–Sen's slope estimator was applied. The results suggested that the post-fire spectral recovery is significantly influenced by the degree of the BS on affected areas. The higher the class of BS, the faster and more extensive the reforestation of the area occurs. About 91% (40,446 ha) of the first 5-year forest recovery after the wildfire belong to the BS classes of moderate and high severity. A regression model showed that land surface temperature (LST) was more significant to post-fire recovery than the variability in precipitation (Pr), explaining about 65% of the variance in post-fire recovery. This study provides new insights into the post-fire forest recovery dynamics and scientific bases for the cost-effective management strategies under changing climate conditions.

Keywords: forest ecosystems; wildfire; burnt area; post-fire forest recovery; Landsat; time-series; GEE; LandTrendr; trend analyses; climatic factors

1. Introduction

Monitoring wildfires and the post-fire forest structural response is increasingly important for understanding their recovery potential, as it strongly impacts ecosystem processes, regional carbon cycling, biodiversity, and climate change [1,2]. It is also crucial for identifying spatial and temporal changes in forest cover and developing nature-based solutions for sustainable forest management [3]. This is particularly significant as large wildfires are becoming more frequent worldwide [4]. Effective monitoring and reliable estimation of post-fire forest recovery in connection with burn severity and climate change indicators [5,6] also can aid in rehabilitation measures and to prevent undesired forest species succession [7,8]. Therefore, research efforts focusing on a holistic understanding of post-fire forest recovery are needed for the professional forestry community.

A recent literature review and critical evaluation indicates that a broad range of studies have been conducted to monitor and assess the spatio-temporal patterns in post-fire forest recovery [9–12]. Most of these studies use satellite images and remote sensing techniques for characterizing and

 doi:10.20944/preprints202409.1781.v

modelling post-fire vegetation recovery at local and regional scales [13–17]. Many researchers utilize multitemporal imagery from sensors like Moderate Resolution Imaging Spectroradiometer MODIS, Landsat-series, SPOT-series, and Sentinel MSI due to their high temporal resolution and free access to archived data [18–21]. Various remote sensing products have been utilised to assess the vegetation recovery trajectories over large territories. This has primarily been achieved by estimating spectral indices, such as Normalised Difference Vegetation Index (NDVI), differenced Normalized Burn Ratio (dNBR), Enhanced Vegetation Index (EVI), Leaf Area Index (LAI), and Fractional Vegetation Cover (FVC) due to their theoretical simplicity and efficiency [22–27]. The use of such spectral indices is ultimately based on establishing pre-fire baselines on the forest cover of remote sensing images in order to compare with the patterns of the post-fire recovery.

Some researchers found that vegetation restoration after the wildfire had a strong correlation with meteorological factors like precipitation and temperature [28–31]. The topography (e.g., slope, altitude, elevation) of forest burnt area may influence surface evapotranspiration following a wildfire, which can also impact the rate of vegetation restoration in various spatial patterns [32–35]. Several studies in modelling of forest recovery trajectories and regeneration rates have been attributed to other significant factors such as species-specific vegetation type, soils, rainfall, and drought indicators [36–39].

Comprehensive studies have shown that forest recovery is heavily depend on the magnitude (burn severity) of the fire regime. In general, the burn severity is typically classified based on the extent of vegetation that is damaged or consumed by the wildfire [40]. A low-severity fire primarily burns the understory vegetation and leaves most of the trees intact, whereas a high-severity fire is akin to a crown fire, which devastates the majority of the trees and other understory species. In ecosystems with mixed coniferous trees, high-severity wildfires often lead to increased post-fire tree mortality, poor regeneration of young trees, contrasting tree cover and it may take decades for forest conditions to fully recover [41–44]. Following a high-severity wildfire, some coniferous ecosystems may not be able to recover to their original state and may shift towards forests with broadleaved species or systems dominated by shrubs [45–47]. Other studies suggest that fire-adapted tree species will actively regenerate after a wildfire of higher severity due to the complete disruption of the overstory forest canopy and loss of apical dominance in the ecosystem [48,49].

Monitoring the state of forest cover requires processing large amounts of geospatial data, which is limited by the available storage and computational resources. Recently, Google Earth Engine (GEE), a cloud-based big data processing platform, has offered users efficient operation and suitability for parallel computing of such data [50]. The platform provides access to a multi-petabyte database of remotely sensed imagery, climate-weather, and geophysical datasets with a series of services, such as web applications, machine learning tools, mapping and visualization of geospatial data [51,52]. Numerous change detection algorithms have been created for the GEE and extensively employed in evaluating forest cover dynamics on an annual time-scale [53–55]. One of this algorithms is the Landsat-based spectral change detection method called Trends in Disturbance and Recovery (LandTrendr), It implements a temporal segmentation approach to divide time-series spectral indices into linear sequential segments [56,57]. Depending on the direction of spectral change, LandTrendr provides annual-scale information about the change event in vegetation cover dynamics by assigning a label of disturbance, recovery, or stable to the given segment [58].

In the last decades, the LandTrendr algorithm has been widely used in different regions to characterize forest disturbances and recovery [59–63]. For example, in western North America from 2000 to 2007, the burnt area recovery varied across different forest types, with intermediate rates in mixed conifer and slowest rates in ponderosa pine stands [64]. In subtropical China, an analysis of forest cover dynamics from 1986 to 2019 using the LandTrendr approach revealed an overall increasing trend. The mean annual forest gain rate was found to be 1.7% [65]. In the Greater Khingan Mountains of China, an integrated approach combining LandTrendr and random forests (RF) models was adapted to track dynamics of forest disturbance and recovery from 1987 to 2021 with an overall accuracy of 0.86 [66]. A LandTrendr time-series analysis conducted over the last 30 years (1990–2020)

 doi:10.20944/preprints202409.1781.v

in humid tropical forests of Madagascar revealed that the main factors influencing disturbance and forest recovery were the complex interactions among biotic, abiotic, and historical land-use data [67].

Several studies have examined the dynamics of forest recovery following wildfires in various ecosystems and regions of the Russian Federation. The majority of these studies were investigated the Siberian forest ecosystems [28,68,69]. The studies have found differences in the sensitivity of forest fire regimes to climate change and forest recovery variability all over the Russian Federation territory. For example, Estimates of NDVI and NBR dynamics in burned ecosystems of North-Central Siberia indicate that the average time for vegetation recovery ranges from 20 to 25 years, with the recurrence of wildfires and high severity significantly prolonging this process [44]. According to other research findings, a substantial shift towards young fire-enduring forests (mainly consisting of birch and aspen) may occur in the southern and mid-taiga regions due to moderate and extreme climate warming, along with increased fire activity [47].

The Middle Volga region, located within the Volga Federal District, is known for its dense forest cover, making it one of the most heavily forested areas in the European part of the Russian Federation (http://www.fedstat.ru, accessed on 16 September 2024). During the last decades this region has experienced rapid changes in forest gains and losses due to intensive forest management (harvesting, intermediate cuttings), reforestation and disturbances (wildfires, droughts, insect and disease outbreaks) [70]. The recent wildfires have various environmental impacts, such as the loss and fragmentation of forest ecosystems, disruption of the hydrological cycle, and negative effects on ecosystem functioning and resilience [71,72]. A detailed monitoring of forest cover in the Republic Mari El conducted as part of the Northern Eurasia Land Cover Dynamics Analysis (NELDA) project (http://www.fsl.orst.edu/nelda/, accessed on 16 September 2024) revealed that approximately one-third (34,228 ha) of the forest area that burned in 2010 were located on pine plantations (*Pinus Sylvestris*) established after a severe wildfire in 1972 [73,74].

Despite a number of the above-mentioned studies, the spatio-temporal distribution of the forest recovery on BAs in the Volga region of the Russian Federation remains understudied. The objective of this study was to examine whether the BS and climate factors (LST and Pr) influence forest recovery. The study combined a Landsat time series NBR with post-fire ground-truth data for a burnt area in the Middle Volga region of the Russian Federation after wildfires that occurred in the years 2002, 2006, 2009, 2010, 2014, 2017 and 2022. The NBR time series covered the post-wildfire period and was combined with pre-fire data to determine potential forest cover conditions before the wildfire. Specifically, the study intended to (I) characterize the spatio-temporal trends and magnitude of the forest recovery over a 20-year period, (II) determine the statistical difference in post-fire forest recovery within three level of the BS, (III) analyse the trends of the forest recovery using a suite of spectral metrics, and (IV) analyse the effect of climatic factors on forest recovery. The trend analysis of the Landsat time series was performed using the advanced Google Earth Engine (GEE) cloud-based platform, applying JavaScript programming through its API (application programming interface).

2. Materials and Methods

2.1. Study Area

The study area encompasses the Middle Volga region of the Russian Federation, including Nizhegorodskaya and Kirovskaya oblasts, as well as the Republics Mari El, Tatarstan, and Chuvashia (ranging between 54.89556 N and 58.08659 N in latitude and 42.47314 E and 51.5 4785 E in longitude; Figure 1). This region is situated in the central part of the East European Plain. According to the national system of silvicultural zones (https://docs.cntd.ru/document/902268260?marker= 6540IN, accessed on 16 September 2024), the northern part of the study area is classified as belonging to the South Taiga region of the European part of the Russian Federation, while the central and southern parts are considered as coniferous-deciduous (mixed) forests (Figure 1).

 doi:10.20944/preprints202409.1781.v

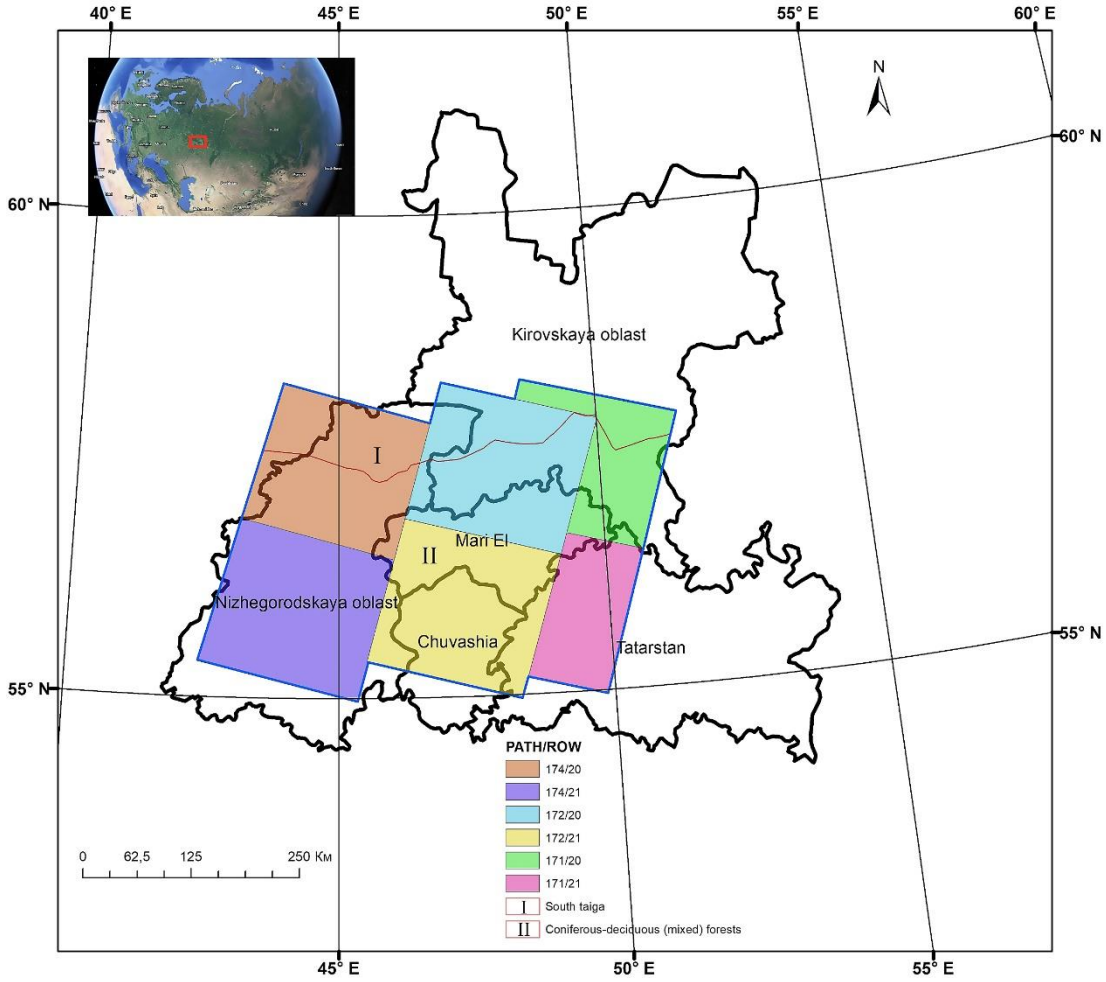

Figure 1. Study area location in western Russian Federation on the Landsat scenes.

The topography of this region is ranging from plains to hilly areas, with elevations ranging from 45 to 316 m above sea level, and the major soil type is podzol. The transition from lower to higher parts is quite gradual. Along the Volga River, there is a central lowland characterised by wide belts of lakes, marshes, and small rivers. The high right bank rises above the valley of the river in the form of a steep ledge with deep ravines [75].

The regio**n'**s climate is classified as moderate-continental, with relatively stable weather during winter and summer, but significant changes in spring and autumn. Summers have been getting hotter, with temperatures in July and August consistently higher over the last 24 years. The mean annual precipitation ranges from 450 to 550 mm, with 250–300 mm falling during the vegetation period (spring and summer). Mean annual temperatures vary from +2.2 °C in the north-eastern part of the region to +3.1 °C in the south-western part, which is favourable for forest growth [76,77]. The eastern part of the Middle Volga generally experiences an increasing trend in land surface temperature and a decreasing trend in precipitation compared to the western part of the region [78].

The main forest types in the region include evergreen coniferous forest, broadleaf (deciduous) forest, and mixed forest. The landscape is predominantly composed of pine (*Pinus sylvestris* L.), birch (*Betula pendula* Roth.), spruce (*Picea abies* Karst.), lime (*Tilia cordata*), and aspen (*Populus tremula* L.). Environmental disturbances such as windstorms, insect outbreaks, and wildfires have become more frequent in the region [77]. In recent decades, due to increased fire recurrence in pine stands, particularly in the Republic Mari El and Nizhegorodskaya oblast, the regeneration of birch and aspen species is common on the burnt sites within the study area. The significant part of broadleaved trees throughout the Middle Volga can be attributed to the increase in birch trees following forest fires in 1921, 1972, and 2010 [73].

 doi:10.20944/preprints202409.1781.v

The study area has historically been subject to a mixed fire regime, with varying levels of burn severity, fire return intervals, and overall fire size. Between 2000 and 2022, forest fires have affected 280,000 hectares or 4% of the total forested area under study in the Middle Volga [72]. The smallest identified wildfire damaged 0.5 ha of forest in Republic Mari El, while the largest identified burned area was 86.6 thousand ha in the Nizhegorodskaya oblast of the region. The wildfire season in the Middle Volga region typically occurred between June and August, with summer lightning storms being a common source of ignition. During this period, the monthly average precipitation was less than 50 mm, the average wind speed was 5 m/s, and the average temperature was 26.4°C. The coniferous forest stands are the most fire-prone ecosystems, accounting for 59.0% of the total burnt area, while deciduous stands account for 25.1%. Insignificant fire occurrences were registered in young forests and shrublands [72].

2.2. Data and Method

2.2.1. Remote Sensing

In our study, the majority of the procedures for image selection, processing, and analysis were conducted on the GEE platform (https://earthengine.google.org/, accessed on 16 September 2024) using JavaScript application programming interfaces. The overall methodology of the research work flow for detecting and analysing the forest recovery over 2000-2023 in the study area using Landsat time-series images and other geospatial data is depicted in Figure 2. The full Landsat Collection 2 Surface Reflectance (SR) archive, including data from TM, ETM+, OLI, and OLI-2 sensors during the summer months (1 May to 30 September), was used to produce annual 30 m composites for the period spanning 2000 to 2023. All necessary Landsat (SR) images were individually retrieved from the following Image Collections stored in GEE: LANDSAT/LT05/C02/T1_L2, LANDSAT/LE07/C02/T1_L2, LANDSAT/LC08/C02/T1_L2, and LANDSAT/LC09/C02/T1_L2. The availability of data for each observed year was verified in GEE by utilizing the buildClearPixelCountCollection code within LandTrendr algorithm [57].

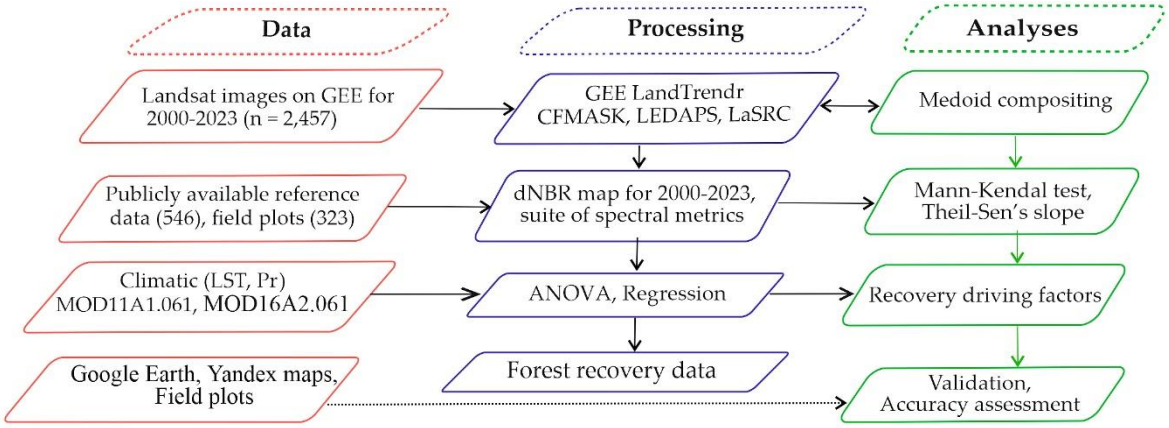

Figure 2. Flow chat of the methodology.

In total, 2,457 Landsat images were acquired during the vegetation period within the study area, covering 6 Landsat scenes (Path 171, 172, and 174; Row 20, 21, Figure 3). This time span (1 May to 30 September) corresponds to the main dry and wildfire seasons in the Middle Volga region [72]. The focus of this study was to investigate the spectral recovery patterns after forest fires that occurred in the years 2002, 2006, 2009, 2010, 2014, 2017 and 2022.

 doi:10.20944/preprints202409.1781.v

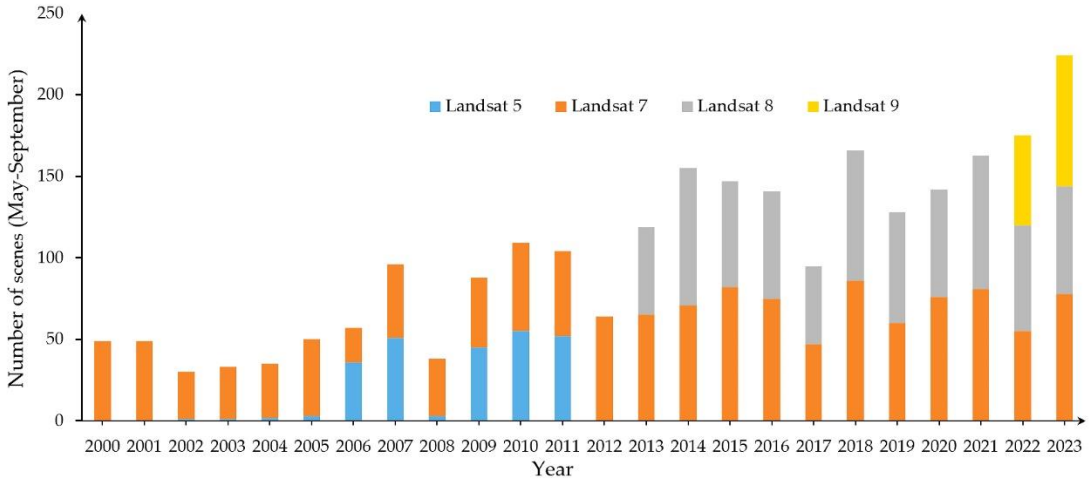

Figure 3. Annual number of Landsat (TM/ETM+/OLI/OLI2) scene observations over the period May–September 2000–2023.

Clouds and cloud shadows were automatically detected and removed from Landsat images with the C Function of Mask (CFMASK) algorithm [79]. The selected images were geometrically and atmospherically corrected and converted to surface reflectance using the Landsat Ecosystem Disturbance Adaptive Processing System (LEDAPS) algorithm for TM and ETM+ [80] and the Landsat 8 Surface Reflectance Code (LaSRC) by the USGS for OLI [81]. To account for the higher 12-bit radiometric resolution of Landsat OLI/OLI-2 compared to the previous ETM+ sensor, an ordinary least squares regression, as reported in Roy et al. [82], was applied to harmonize linear differences between the spectral values of both instruments and normalize the reflectance.

2.2.2. Climate Data

The simulated climate data for the Middle Volga region over the period 2000–2023 (May to September) were acquired from various gridded datasets (Table 1). Two meteorological data products were selected for use in the study. The MOD11A1.061 Terra Land Surface Temperature and Emissivity Daily Global archive datasets was used to estimate the average monthly land surface temperature (LST) values in Celsius (^{0}C) at 1-km spatial resolution. The Global Precipitation Measurement (GPM) IMERG (Integrated Multi-satellitE Retrievals for GPM) Final Precipitation L3 Half Hourly 0.1^0 x 0.1^0 V06 (GPM_3IMERGHH) product was used to determine the gridded monthly average precipitation (Pr) values in the studied region (https://giovanni.gsfc.nasa.gov/giovanni/ accessed on 16 September 2024) (Table 1). We downloaded the data through the GEE platform using the projection coordinate system set to "EPSG:32638/39".

Table 1. Data employed for estimation of vegetation recovery and climatic factors monitoring in the Middle Volga region from May to September 2000-2023.

No	Purpose	Data, Product ID	Scale	Source
1	Monitoring of vegetation recovery	Landsat time series	30 m	https://earthengine.google.com/
2	Land Surface Temperature	Monthly MODIS/061/MOD11A1	1 km	MOD11A1.061 Terra Land Surface Temperature and Emissivity Daily Global ee.ImageCollection
3	Precipitation	Monthly GPM_3IMERGHH	0.1^0 x 0.1^0	https://giovanni.gsfc.nasa.gov/giovanni/
4	Validation, accuracy assessment	Google Earth Yandex maps	10-30 m	www.googleearth.com https://yandex.ru/maps

 doi:10.20944/preprints202409.1781.v

5		Field plots of Volgatech	90x90 m

2.2.3. Burn Severity

To examine the relationship between forest recovery and climatic factors (LST and Pr), we converted the selected pixels of the time series into a NBR. Burn severity (BS) across a range of wildfires in the Middle Volga region was estimated on the base of dNBR values. The classification into low- (50-190), moderate- (200-360), and high-severity (> 400) dNBR classes [83] was carried out at the pixel-level and averaged for each estimated burnt area. To improve the detection of early signs indicating potential forest recovery in the study area, the Landsat time series data were filtered to only include spectral recovery trajectories from low, moderate and high severity classes (Figure 4). The burnt areas were selected using a threshold value of > 50 dNBR, which represented a level of severity high enough to initiate the growth of a young trees.

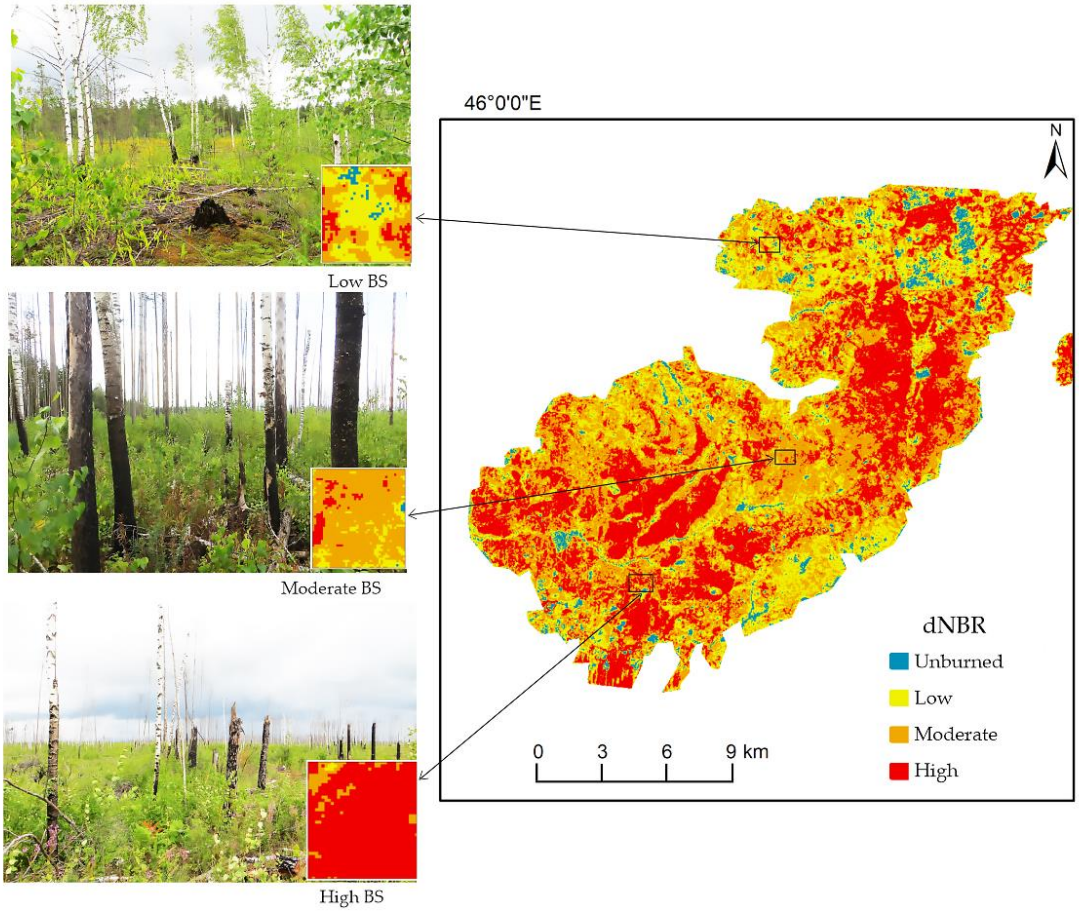

Figure 4. Examples of forest recovery in three different burn severity sites of the 2010 wildfires in Middle Volga region.

2.2.4. LandTrendr Algorithm

To analyze the vegetation recovery dynamics on burnt forest areas, we used the LandTrendr algorithm in the GEE platform to process the prepared time series Landsat images. We applied a medoid selection process [84] to the stack of Landsat images, which is a multi-dimensional equivalent of the median. The medoid technique compares the spectral values of each estimated image to the median spectral values of each pixel across all visible and infrared bands in all available Landsat time series images. The pixel with the minimum sum of squared differences between observations and median spectral values was then selected by LT, using Euclidean distance. This approach enabled us to minimize the data volume in GEE, reduce atmospheric impact, and mitigate sensor influences to

 doi:10.20944/preprints202409.1781.v

the greatest extent possible. As a result, we obtained an aggregated stack of Landsat images for a 23-year time series, with interpolated spectral values and reduced year-to-year noise.

2.2.5. Spectral Forest Recovery Metrics

To estimate the rate and patterns of forest recovery in the region we used a suite of spectral metrics (Figure 5) (Table 2). The recovery metrics were developed using trend-fitted NBR values from the Landsat time series analysis. A five-year post-fire period was chosen to examine spectral forest recovery in the Middle Volga, as this time frame has been identified as crucial for monitoring forest regrowth in many previous studies [38,65,92,93].

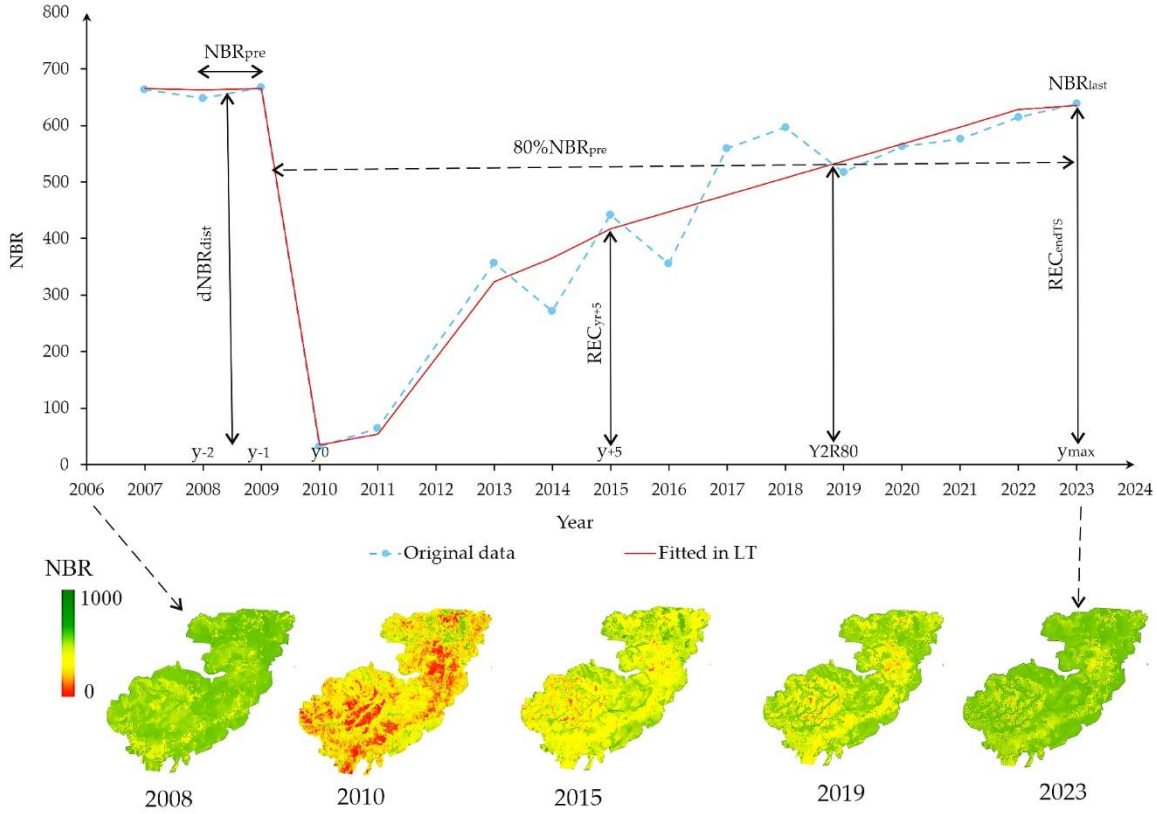

Figure 5. Schematic of spectral recovery metrics for the burnt area of the 2010 forest fire, using an example of a fitted NBR trajectory in the LandTrendr program.

Table 2. Spectral metrics used for monitoring of the forest recovery.

No	Spectral metric	Calculation	Description	Reference
1	Absolute Recovery Indicator	$RRI=ARI/dNBR_{dist}*100$; $ARI = NBR_{y+n} - NBR_{y0}$	A relative measure of short-term recovery; NBR_{y+n} and NBR_{y0} correspond to the NBR value n years after and year of the wildfire.	[12,40]
2	Relative Recovery Indicator	$YrYr= (NBR_{ymax} - NBRyo) / Y_{max}$	Average rate of spectral change from the year of fire to the max year of the recovery; NBR_{ymax} – maximum value of NBR at Tmax (year of max recovery).	$dNBR_{dist}$ - change in NBR due to the wildfire. NBR average of 2 years prior to wildfire (y-2 and y-1).	[12,62,91,93] [12,62,93]
4	Year to Recovery of 80 Percent	$Y2R80= NBR_{y+n} / 0.8*NBR_{pre}*100$	Recovery when NBR reach 80% of the NBR_{pre} value	[91–93]
	Year On Year Average			[12]
	NBR prior to wildfire	$NBR_{pre} = (NBR_{y-2} + NBR_{y-1}) / 2$		

 doi:10.20944/preprints202409.1781.v

Recovery at the end of TS	$Rec_{endTS} = (NBR_{last} - NBR_{y0}) / (dNBR_{dis})*100$	Spectral recovery observed at the end of the estimated time series.	[62]

To minimize the effects of inter-annual variation due to atmospheric effects or other noise sources, we used a pre-fire 2-year window for calculating NBR prior to wildfire (Figure 5). The change in NBR five years after the wildfire was used as the Absolute Recovery Indicator (ARI) (Table 2). Essentially, this metric indicates the degree of change in the NBR value for a given Landsat pixel has over the 5-year period following wildfire. Another metric used is the Relative Recovery Index (RRI), which enables the description of regrowth rates over time or for each successional stage, defined by the number of investigated segments [12,91].

The Years to Recovery of Eighty Percent (Y2R80) represented the number of years required for a disturbed pixel to reach 80% of the pre-disturbance NBR value (Figure 5). In the context of this study, meeting 80% of the pre-fire NBR value indicates a positive trend in the return of vegetation to the burnt area. However, it does not necessarily signify a return to the same forest cover characteristics that were at a site prior to the wildfire. This is particularly relevant for coniferous and broadleaf tree species growing in the Middle Volga region, such as pine stands that typically reach maturity in 60-80 years and birch trees that reach maturity in 30-40 years.

The Year on Year (YrYr) metric offers an understanding of the average annual change in NBR values after wildfire and provides insight into the annual post-fire recovery of vegetation. A YrYr value of zero indicates that no forest recovery had occurred in the burnt area, while positive values indicate the average increase in NBR during the estimated years that followed the wildfire event.

An important indicator that takes into account the longer duration of regrowth in burnt area is the spectral recovery observed at the end of the time series (Rec_{endTS}) [62]. Since our Landsat time series covered a period of over two decades, and the majority of the burnt areas were possibly to have spectrally recovered by the 2023, this metric can be useful in indicating areas that are experiencing delayed recovery.

2.2.6. Reference Data Collection and Validation

To validate the burn severity and estimate the accuracy of the forest recovery trend analyses, we randomly selected 843 forest BA test sites at each phase of vegetation recovery from 2000 to 2023 for the investigated territory of the Middle Volga region. To identify these sites, we used publicly available Google Earth and Yandex Maps platforms and the visual interpretation method [94]. The accuracy assessment of the forest recovery by BS classes was carried out through visually assessing vegetation cover in randomly distributed sample plots all across the investigated BAs.

Additionally, to support the remote sensing analysis, several field campaigns were conducted by the Volgatech team during the summer period (June-August) of 2011, 2012, 2014, 2017, and 2019-2024 in the burned areas of the Middle Volga. The team established 386 sample plots that represented a variety of stand ages, tree species, and typical forest ecosystems grown in the region. The selection of sampling locations ensured that all possible levels of BS would be covered. To measure BA and BS, the composite burn index (CBI) was used [40,83]. The sample plots were randomly distributed, mainly in conifer and mixed broadleaved stands within the BAs.

The geographical coordinates of all sites were recorded for each sample plot using a GPS, with a minimum size of 90 by 90 meters. Within each sample plot, the team measured tree species composition, diameter at breast height (DBH), tree height, crown base height, and scorch height. The fieldwork was also conducted on existing field plot locations, where the team measured forest regeneration (number of seedlings and re-sprouted shrubs), late survival rate, and soil condition. To increase the accuracy for training and validation, only the grid cells at the center of each plot were selected, rather than the entire plot.

2.2.7. Trend Analysis

A Mann-Kendall (MK) nonparametric statistical test was employed to quantify the temporal trend of the estimated factors based on the Landsat time series [85,86]. The rate of the change and

 doi:10.20944/preprints202409.1781.v

magnitude of the estimated factor's trends were assessed by means of the Theil-Sen's slope estimator, a non-parametric technique for assessing the median slope [87,88]. A Mann-Kendall test is usually conducted to determine whether a time series exhibited a statistically significant monotonic increasing or decreasing trend ($p < 0.05$). Non-significant trends were considered unimportant and were excluded from further analysis, although their Theil-Sen slopes are still presented in the results for the sake of completeness. Both of these tests, which the World Meteorological Organization has recommended for application in climate studies, are widely used in trend analyses [89,90].

3. Results

3.1. Burn Severity

We have complied the results from the BS analysis based on the dNBR for the estimated burnt areas of the 2002, 2006, 2009, 2010, 2014, and 2018 forest fires in Table 3. The BS classes obtained as a result of the analysis in GEE over the study area were categorised into 4 groups based on their size: less than 50 ha, 50-200 ha, 200-1000 ha, and more than 1000 ha. The establishment of these groups was based on an even distribution of the number of each BS class with the corresponding area in each group.

Table 3. The distribution of BS classes on the burnt area in the Middle Volga region for 2002-2018.

Burn severity class	Class boundary, dNBR	Area, ha/%	BS groups by area, ha/%			
			< 50	50 – 200	200 – 1000	> 1000
Unburned	< 50	4998/1.9	908/42.9	1377/27.8	1240/8.4	1473/0.6
Low	50 – 200	32871/12.6	534/25.2	1155/23.3	3556/24.1	27626/11.5
Moderate	200 – 400	112433/42.9	430/20.3	1427/28.8	5724/38.7	104853/43.7
High	> 400	111511/42.6	243/11.5	997/20.1	4256/28.8	106015/44.2
Disturbed		256815/98.1	1207/57.1	3579/72.2	13536/91.6	238494/99.4
Total		261813/100	2115/100	4956/100	14776/100	239967/100

The largest area according to the GEE falls on the moderate (112433 ha or 42.9%) and high (111511 ha or 42.6%) BS classes (Table 3). Considering that aboveground vegetation from the moderate class was also generally severely damaged during the wildfires, we can assume that approximately 86% of the forest cover was completely destroyed on the studied BA. Taking into account all three groups of the BS (low, moderate and high), approximately 98% of the burnt areas were disturbed after the wildfires. The remaining 1.9% of the unburned trees present small fragmented patches all over the BA. These trees provide seeds for the natural forest recovery and help maintain biodiversity of the ecosystem.

In burnt areas of less than 50 ha and from 50 to 200 hectares, the largest share is occupied by areas with a dNBR of less than 50 (42.9%/908 ha and 27.8%/1377 ha). The area with a low degree of damage occupies from 11.5% (in BA over 1000 ha) to 24.1% (in BA 200 – 1000 ha). The area covered in the group of more than 1000 ha by the moderate (43.7% or 104853 ha) and high (44.2% or 106015 ha) severity classes was almost equal. Approximately 99% or 256,8 thousand ha of the disturbed forest areas were in the group of more than 1000 ha category.

3.2. Statistical Comparison of the Spectral Metrics

A multiple sample comparison test was conducted for the RRI5, YrYr, and YrYr5 spectral recovery time series datasets. The ANOVA test showed a statistically significant difference between the means of the RRI_5 low burn severity values and the RRI_5 moderate and high BS values at the 5% significance level (F-ratio=37.61, p-value=0.00). On the other hand, there was no statistically significant difference (F-ratio=2.52, p-value=0.14) between the means of the RRI_5 moderate and RRI_5

 doi:10.20944/preprints202409.1781.v

high BS variables. The mean RRI_5 for the moderate severity recovery group was 18.0, compared to 18.6 for the RRI_5 high severity recovery (Figure 6a).

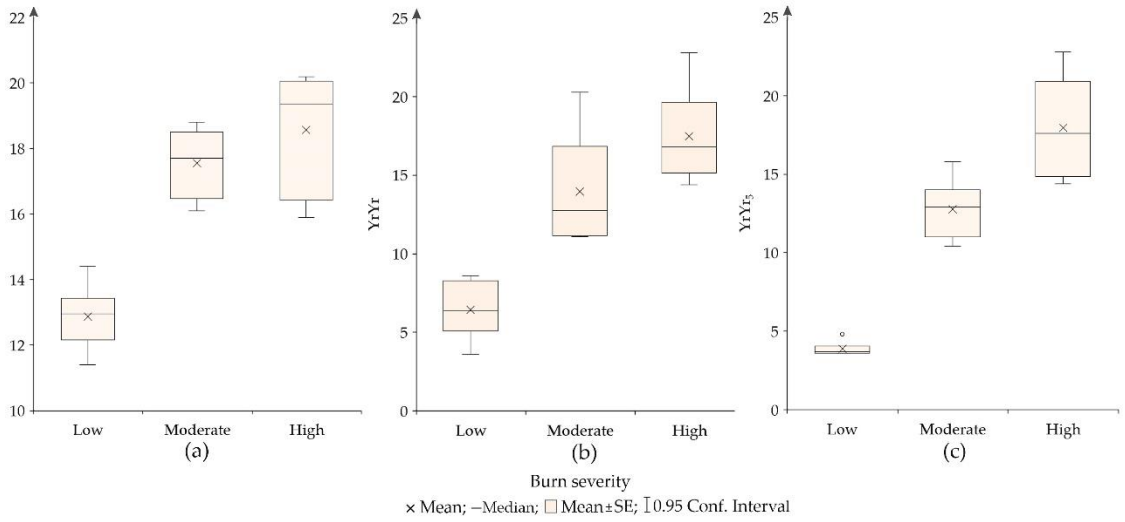

Figure 6. Box-and-Whisker plot of the time series recovery metrics by the three burn severity classes: (a) relative recovery indicator at 5 years after the wildfire (RRI_5); (b) average annual recovery (YrYr), (c) annual recovery at 5 years after the wildfire ($YrYr_5$).

The ANOVA test indicated a statistically significant difference between the means of the three classes of YrYr BS values at the 5% significance level (F-ratio=62.14, p-value=0.00). The average mean YrYr for the low severity recovery class was 6.5, compared to 14.0 for moderate recovery, and 17.5 for the high severity BA (Figure 6b). The statistical difference between the three classes of BS was even more apparent when the $YrYR_5$ metric was compared in the ANOVA at the 5% significance level (F-ratio=22.97, p-value=0.00). The average mean $YrYr_5$ during the first five years after the wildfire for the low severity recovery calss was 3.9, compared to 12.8 for moderate recovery, and 18.0 for the high severity BA (Figure 6c).

The statistical analysis of the spectral metrics revealed that the recovery in different BAs is directly influenced by the degree of burn severity. The higher the class of wildfire disturbance, the faster and more extensive the reforestation of the area occurs.

3.3. Vegetation Recovery Following Wildfire

As shown in Figure 7, the NBR values decreased below the normal forest growth after the wildfires that occurred in 2002, 2006, 2010, and 2018, and the extent of this decline varied with the burn severity. Under the three BS classes, the NBR index values have exhibited similar forest recovery trends for all estimated BA. The majority of estimated BA show an increase in RRI_5 metric values during short term recovery (Figure 7). In the first 5 years following wildfire, the areas with all three classes of BS had an RRI_5 value of 44,533 ha or 17.3% of disturbed area (excluding unburned BS class) (Table 4). On average, 40.8% (18,164 ha) and 50.0% (22,282 ha) of the RRI_5 areas belong to the BS classes of moderate and high severity, which are considered indicative of spectral forest recovery (Table 4). In low-severity BA, the RRI_5 was sufficiently lower at 9.2% (4086 ha). This could be attributed to minimal disturbance to canopy and ground cover during the wildfire, resulting in less impact on the regeneration of the BA.

 doi:10.20944/preprints202409.1781.v

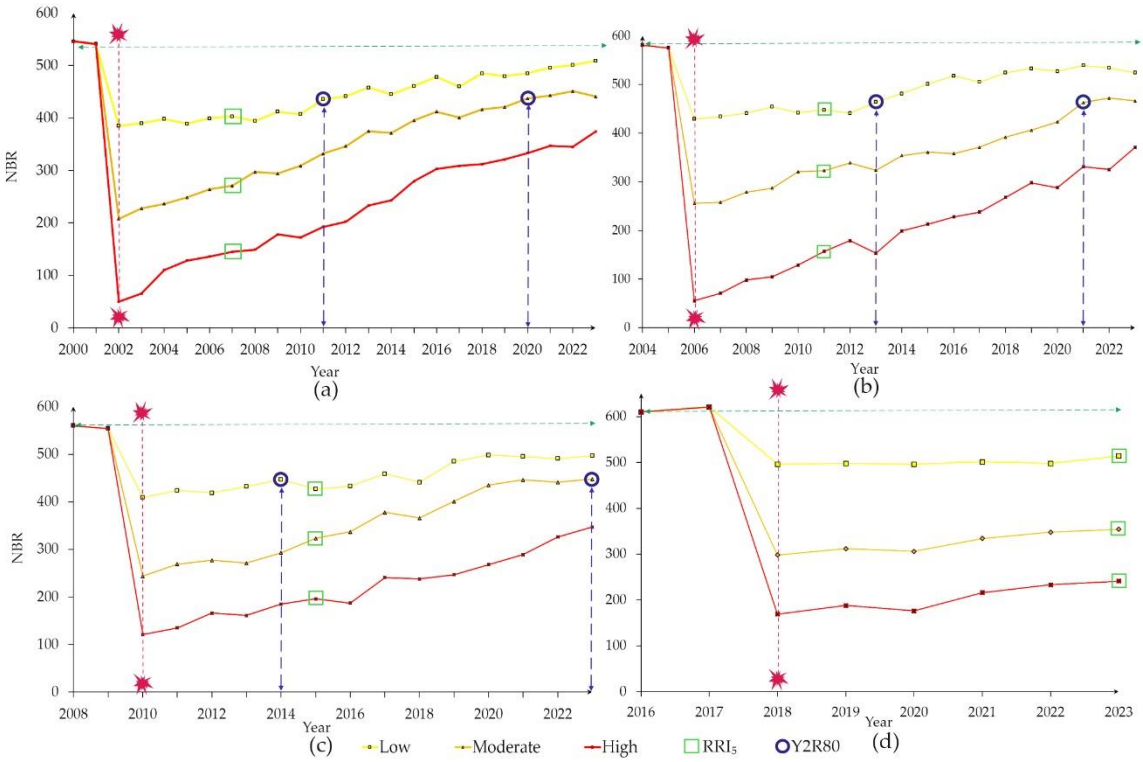

Figure 7. Time series of NBR recovery by burn severity after the wildfires: (**a**) 2002; (**b**) 2006; (**c**) 2010; (**d**) 2018. The green horisontal dashed line represents the mean NBR reference for the two years prior to the wildfire, and the red veritcal dashed line marks the year of the wildfire.

Only 13.1% (33,755 ha) of the disturbed area reached the Y2R80 metric for the low and moderate BS classes during the estimated time series (Table 4). In general, Y2R80 reached its target value within 4 to 8 years after the wildfire in areas with low BS, and within 14 to 18 years in areas with moderate burn severity (Figure 7 a,b,c). During the period from 2002 to 2023, the forest recovery to the Y2R80 level primarily occurred in areas (72.2%) with low burn severity (Figure 8b).

Table 4. Forest recovery area during 2002-2023 years by burn severity based on spectral metrics.

Spectral metric	Recovery area by BS, ha/%			Total, ha	% of disturbed area
	Low	Moderate	High		
RRI_5	4,086/9.2	18,165/40.8	22,282/50.0	44,533	17.3
Y2R80	24,379/72.2	9,376/27.8	-	33,755	13.1
Rec_{endTS}	19,823/13.0	73,833/48.6	58,357/38.4	152,013	59.2
YrYr	417/6.0	3,136/44.8	3,451/49.2	7,004	2.7
$YrYr_5$	198/3.1	3,153/49.3	3,024/47.6	6,357	2.5

 doi:10.20944/preprints202409.1781.v

Figure 8. On site examples of three recovery stages on BA of the high BS for the spectral metrics: (a) RRI_5; (b) Y2R80; (c) Rec_{endTS}.

The BA with a moderate and high BS levels have the highest values of the Rec_{endTS} metric. In the moderate BS class, the Rec_{endTS} reached 73,833 thousand ha (48.6%), while the high BS areas covered 58,357 ha (38.4%) of the total calculated by the end of estimated time series. The remaining 19,823 ha (13.0%) of BA was recovered during the period from 2002 to 2023 on the areas of low BS. These figures suggest that in all three classes of BS the forest is naturally recovering sustainably.

During the estimated period, the post-fire YrYr recovery metric was estimated annually at 2.7% of the total disturbed area by the wildfire. In low severity BAs, the YrYr constituted 417 ha (3.1%), while at moderate and high BS levels, it was 3,136 (44.8%) and 3,451 (49.2%) respectively (Table 4). The 5-year post fire YrYr5 metric showed a slightly lower recovery rate of 2.5% of the disturbed area, particularly in the low severity BAs. Meanwhile, the YrYr5 in the moderate and high severity areas were almost similar to the annual YrYr values (Table 4). Ultimately, by the end of the study period from 2002 to 2023, the majority of BAs (about 60%) in the Middle Volga region that were disturbed by wildfires had shown positive trends in forest recovery (Figure 8 a,b,c).

3.4. Spatial Analyses of Forest Recovery

Based on the Mann–Kendall τ (tau) correlation coefficient and Theil–Sen's slope (TSS) analysis, the trend of forest recovery on a pixel scale was analysed for the burned area during the vegetation season in the Middle Volga region over the period 2003–2023 (Table 5). The results of natural forest regeneration trends over 20 years show diverse spatial variations. Figures 9 and 10 show the monotonic trends of tau and TSS in the Landsat time series for the forest recovery (NBR), highlighting areas with an increasing trend (in green) and a decreasing trend (in red). As shown in the Figure 9, a stable trend towards forest recovery is observed in the three largest BAs within the study area. This trend is particularly evident in areas with moderate and high BS. In general, for the study area, the

 doi:10.20944/preprints202409.1781.v

NBR exhibits an increasing trend over an area of 31,421 ha for low BS, 109,265 ha for moderate BS, and 106,969 ha for high BS. The Mann-Kendall trends with tau < 0, which indicate a decrease in forest cover during the study period, reach 14.1% for low BS, 2.5% for moderate BS, and 3.2% for high BS sites.

Table 5. Post-fire natural forest recovery trends in the Middle Volga, based on the Mann-Kendall's test for BAs with different burn severity and statistically significance values ($p < 0.05$). The data are presented in ha and percentages in relation to the total disturbed area in the period 2002–2023.

M-K tau	Burn severity class, ha/%		
	Low	Moderate	High
-1 – 0	1450/14.2	3167/2.5	4542/3.2
0 – 0.4	6640/18.4	15981/13.6	16836/14.8
0.41 – 0.8	22871/72.2	80794/72.7	72115/65.5
0.81 – 1.0	1910/5.2	12490/11.2	18017/16.5
Total	32871/100	112433/100	111511/100

In terms of the magnitude, all three BS classes show mostly a positive Theil-Sens's slope in forest recovery across areas disturbed by wildfire (Figure 11). The majority (73%-93%) of significant slopes (p-value < 0) range between 10 and 30, with an average yearly increase of 4.6 in low, 4.3 in moderate and 3.6 high BS areas throughout the time series.

The increasing trends of the forest recovery are not clustered in a specific area; their distribution is regular across the BAs of the study territory. The majority of negative trends are represented in the form of small patches, including sites than burned two or even three times during the investigated period [72]. Most of such patches are located on the area of small BAs in the Republic Mari El and Nizhegorodskaya oblast of the Middle Volga region (Figure 9,10). Overall, the results of using Mann-Kendall and Theil-Sen's slope estimator statistical tests showed consistency in the detection of spatio-temporal trends for the forest recovery variables in all BS classes.

 doi:10.20944/preprints202409.1781.v

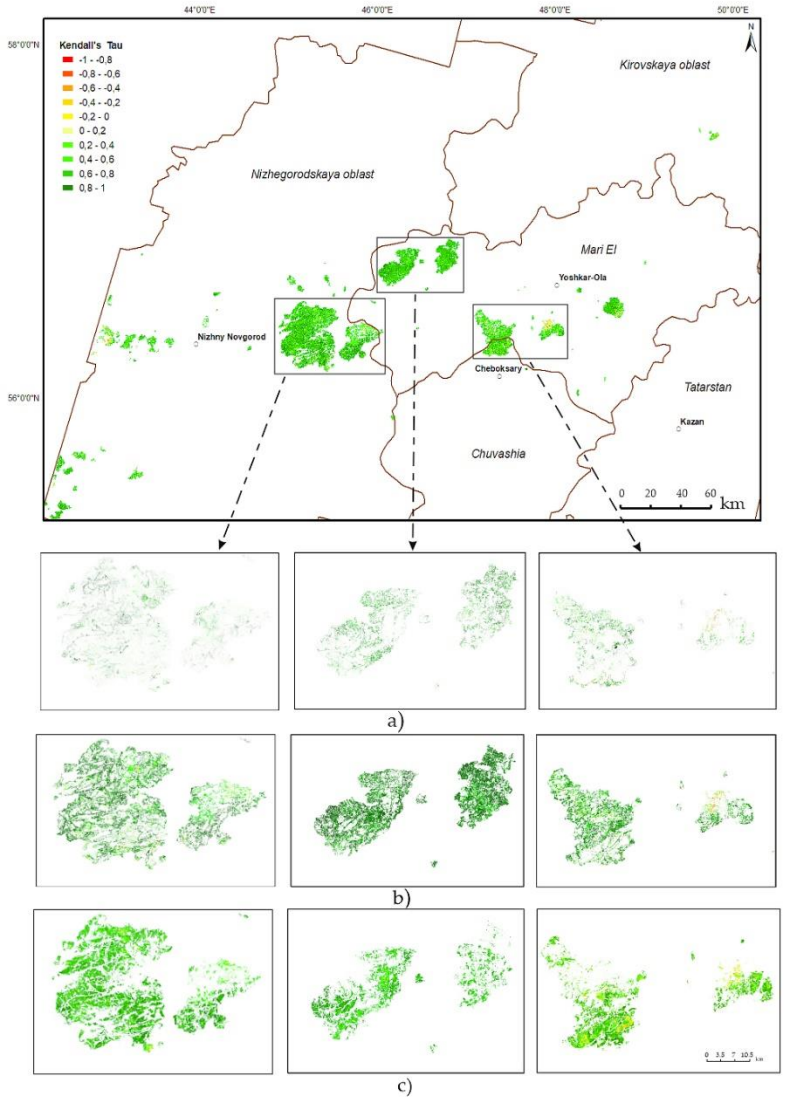

Figure 9. Spatial trends of post-fire natural forest recovery in the Middle Volga region (2003–2023) based on the Mann-Kendall's Tau test ($p < 0.05$) for sites with different burn severity: a) low; b) moderate, c) high.

 doi:10.20944/preprints202409.1781.v

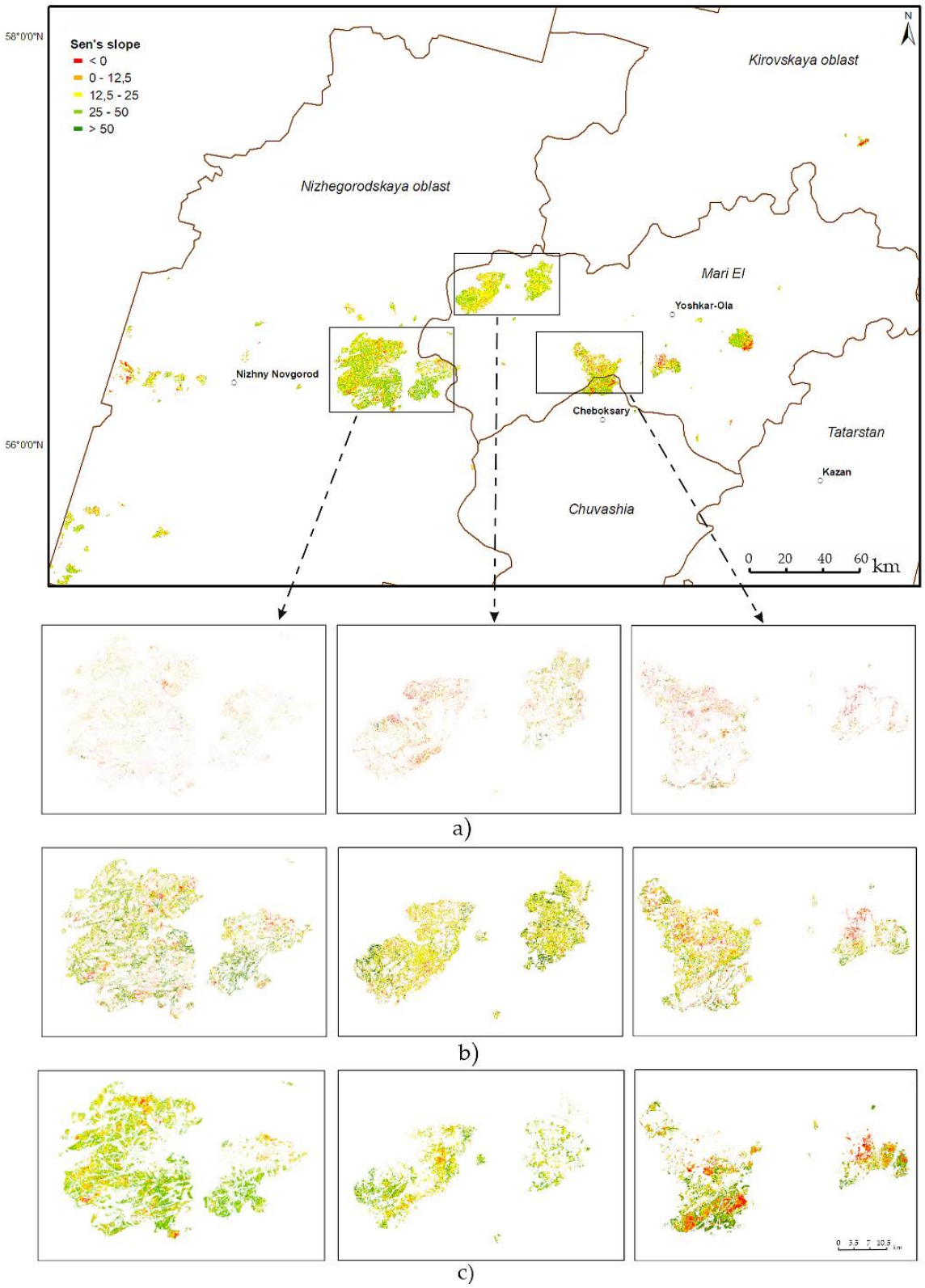

Figure 10. Spatial trends of post-fire natural forest recovery in the Middle Volga region (2003–2023) based on the Theil-Sen's slope ($p < 0.05$) for sites with different burn severity: a) low; b) moderate, c) high.

 doi:10.20944/preprints202409.1781.v

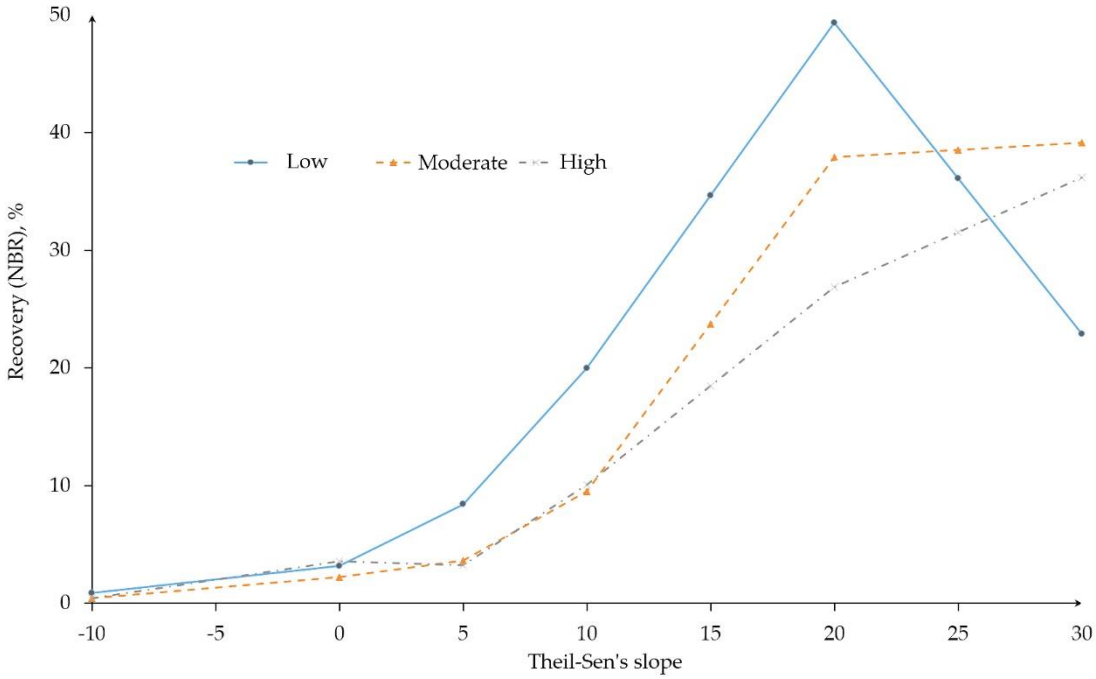

Figure 11. The Theil-Sen's slope (magnitude) trend for forest recovery in the Middle Volga region from 2003-2023 for sites with different burn severity.

3.5. Assessing the Impact of Climate Factors on Forest Recovery

To explain the influence of burn severity and climatic variables on forest recovery (NBR dynamics), multiple linear regression analysis was used. The analysis covered a period of 5 years of intensive recovery and additional 10 years after the wildfires, during which low- and moderate burned areas reached 80% forest recovery. Two important climate variables were derived from MODIS imagery and the GPM_3IMERGHH NASA product to model post-fire recovery. The results from the multiple linear regression analysis for forest recovery at different BS sites were summarized in Table 6. The best equation with the highest fit of combined climatic factors considered was the one using the monthly mean of LST and Pr averaged over the estimated period (May to September). All of the estimated climate variables for predicting the recovery during both periods were statistically significant at the 95% level (P-value < 0.05).

Table 6. The results of the multiple linear regression model for forest recovery (NBR) at different burn severity sites. P-value < 0.05.

Burn severity	Variable	Estimate	Standard error	T-statistic	R^2, %	F-ratio
5-year period after a wildfire						
Low	Constant	307.69	69.491	69.491	60.0	410.39
	LST	4.847	28.545	28.545		
	Pr	0.046	1.828	1.828		
Moderate	Constant	124.978	6.987	17.886	56.5	354.05
	LST	6.878	0.265	25.899		
	Pr	-0.251	0.039	-6.318		
High	Constant	-45.696	10.377	-4.404	60.6	471.03
	LST	8.896	0.319	27.844		
	Pr	-0.181	0.068	-2.638		
5+10-year period after a wildfire						
Low	Constant	231.066	11.697	19.755	64.9	758.47
	LST	10.098	0.386	26.131		

 doi:10.20944/preprints202409.1781.v

	Pr	-0.715	0.050	-14.187		
Moderate	Constant	18.549	18.549	-6.786	66.7	878.24
	LST	0.608	0.608	32.935		
	Pr	0.081	0.081	-8.212		
High	Constant	-179.571	20.374	-8.814	62.7	738.57
	LST	19.399	0.675	28.733		
	Pr	-0.316	0.019	-16.144		

The multiple regression analyses showed that climatic factors played an important role in the BA forest recovery during the investigated period. Values of both the standard error statistics (SE) and T-statistic indicate that among the climatic variables, temperature (LST) had a stronger impact on the forest recovery (vegetation growth) compared to precipitation (Table 6). LST was found to be an important factor in both the estimated time periods (Figure 12, 13).

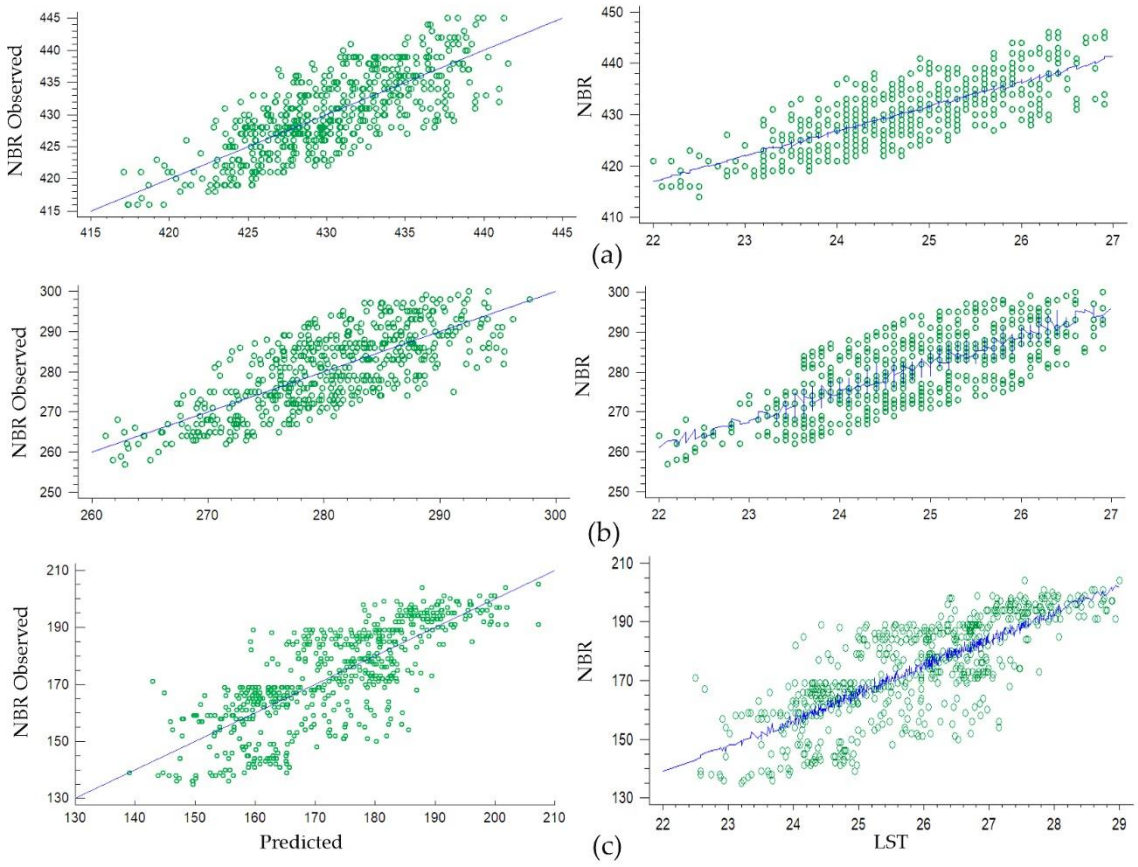

Figure 12. The fitting results of a multiple linear regression model to describe the relationship between the natural forest recovery (NBR) during 5 years from a wildfire, the land surface temperature (LST), and the precipitation (PR) for sites with different burn severity: a) low; b) moderate, c) high.

 doi:10.20944/preprints202409.1781.v

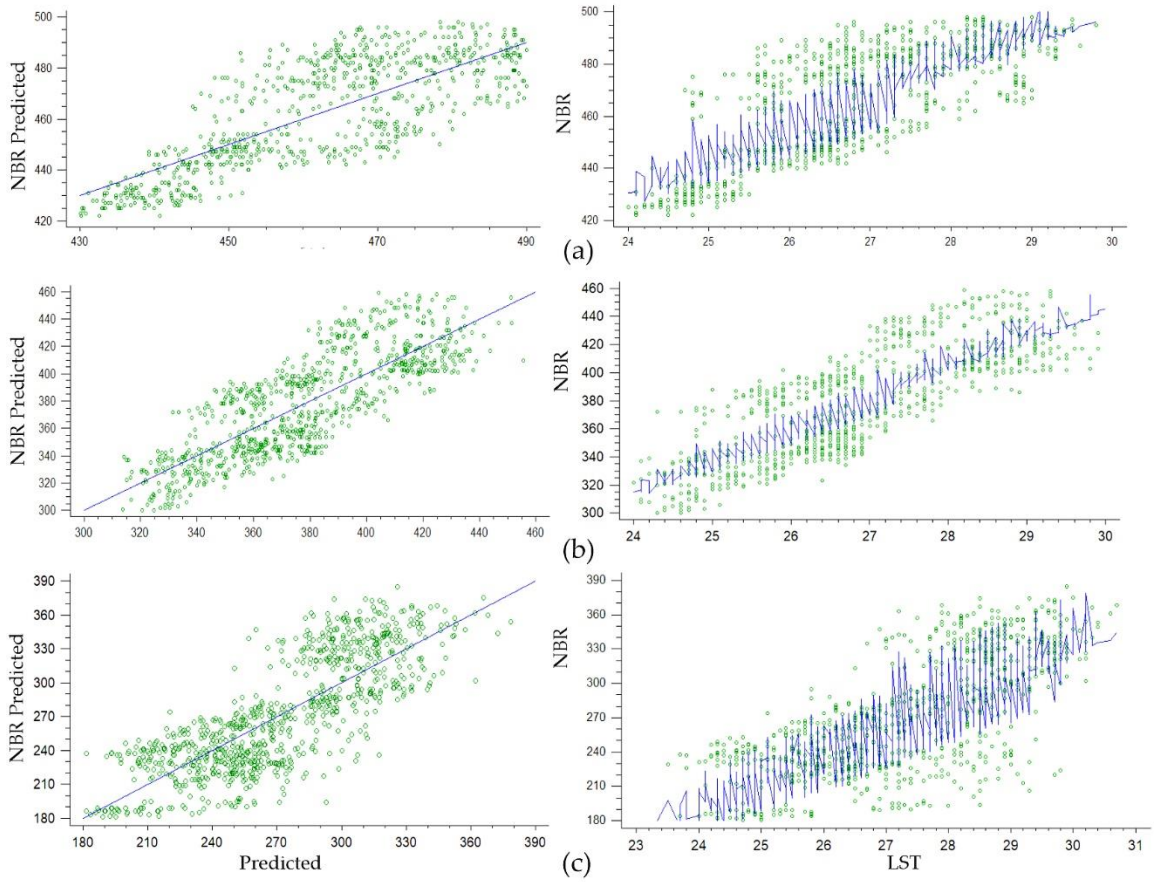

Figure 13. The fitting results of a multiple linear regression model to describe the relationship between the natural forest recovery (NBR) during 5+10 years from wildfire, the land surface temperature (LST), and precipitation (PR) for sites with different burn severity: a) low; b) moderate, c) high.

The precipitation data generally showed a weaker, negative influence on the forest recovery. However, since the p-value for Pr in all equations is less than 0.05, this variable is statistically significant at the 95% confidence level. Consequently, this variable was retained in the model. The models, with a fitted R^2 statistic for the 5-year period varying from 56.5% in the moderate and 60.6% in the high BS area, indicate that the combined climatic factors of LST and Pr significantly influence the forest recovery in the investigated region (Table 6, Figure 12). The same patterns shown for the regression results of BA with 5+10-year period after a wildfire. During the 5+10-year period, the strongest relationship of the forest recovery with the climate factors was shown in the moderate BS area, with a fitted R^2 statistic reaching 66.7% in the model (Table 6, Figure 13).

4. Discussion.

Wildfires have a severe impact on tree cover, the forest carbon budget, and ecosystem services, particularly in the coniferous-deciduous (mixed) forests of Western Russian Federation, where large areas of forest ecosystems are burned annually. A better understanding of the spatial patterns and underlying factors that drive tree recovery in areas affected by wildfires is essential for developing effective forest management strategies and climate change mitigation. Numerous previous studies have demonstrated that the use of remote-sensing images and cloud-based processing platforms provide a cost-effective and efficient way to monitor the recovery of vegetation after wildfire events.

In this study, we investigated the effect of burn severity on the natural forest recovery process in the Middle Volga region by analysing various NBR spectral metrics derived from Landsat images using the GEE and the LandTrendr algorithm. The NBR time series were compared with data on post-fire climate conditions over the investigated area and three classes of burn severity. This allowed us to characterise potential factors influencing the forest recovery processes and to determine their

 doi:10.20944/preprints202409.1781.v

short-term spatio-temporal trends. Field survey data were also utilised to identify the tree species present on the BAs, their combinations, growth conditions, and sources of variability in the recovery processes that are not seen from the Landsat imagery data alone.

We found that the use of time series analysis of Landsat data, employing the LandTrendr segmentation algorithm, has been an effective tool for tracking the gradual spectral recovery processes of trees over a large forest area after wildfires. The results showed that the forest recovery during 2003-2023 period in the Middle Volga region was highly variable and dependent on the burn severity within the BAs. The research findings indicated that annual rates of spectral forest recovery consistently increased over time after the wildfires that occurred in 2002, 2006, 2010, and 2018, and the magnitude of this increase varied with the burn severity across the entire investigated BAs.

The ANOVA test generally confirmed the statistically significant difference between the means of the RRI5, YrYr, and YrYr5 spectral metrics for low, moderate, and high BS classes at the 5% significance level. This revealed that the forest recovery on the estimated BAs is directly influenced by the degree of burn severity. The higher the class of disturbance, the faster and more extensive the reforestation of the area occurs, which supports former studies with the similar conclusions [60,64]. Mostly, the forest recovery rates of NBR spectral metrics were highest shortly after the wildfire, slowly stabilising by the end of time series analyses (Figure 6). The BAs with the highest burn severity had a more extensive rate of forest recovery within the first five years after the fire, which is also consistent with the previous studies [16,29,43,46]. About 91% (40,446 ha) of the RRI5 belong to the BS classes of moderate and high severity. During the 2002-2023 period, the post-fire YrYr recovery metric annually reached 2.7% of the total BAs.

The visual inspection of the BAs and validation plots suggests that the recovering vegetation primarily comprises of deciduous pioneer species such as birch and aspen. Such mixed, highly dense forest ecosystems are common in the Middle Volga region [73,77]. The recovery of Scotch pine is also confirmed on the validation site plots, particularly on sandy soils during 5-15 years after the wildfire. The ongoing succession processes on the BAs in the Middle Volga region, following several severe wildfires, include an extensive shift toward forests dominated by broadleaved deciduous and mixed stands. It is important to consider these factors in the post-fire management strategy to take necessary measures to mitigate the danger of wildfires in the region.

The use of the NBR spectral metrics allowed us to compare the recovery of the BAs in relation to their pre-fire conditions. The results of this study demonstrate that only 13.1% (33,755 ha) of the BAs reached the Y2R80 metric for the low and moderate BS classes during the 20 years after the wildfire (Table 4), mostly in deciduous forest ecosystems. The forest recovery to the Y2R80 level primarily occurred in areas (72.2%) with low burn severity (Figure 8b). This aligns with the minimum recovery intervals of 15 years for broadleaved and 25 years for the coniferous species to consider them recovered after the wildfire.

In order to quantify the spatio-temporal patterns of forest recovery, we carried out the Mann–Kendall trend analysis for the periods of 2003–2023. The analysis revealed primarily increasing NBR trends at the pixel level for all three classes of BS, especially in BAs with moderate (97.5%) and high (96.8%) severities. In contrast, decreasing Mann-Kendall trends in forest cover were observed mostly in low (14.1%) BS areas in the form of small patches. The validation plots showed that these negative trends in the time series largely corresponded to areas that lost tree dominance after the wildfire, transitioning to marshlands or becoming dominated by grasses and shrubs. Some decreasing Mann-Kendall trends were also found covering BAs across the vast territory of the Middle Volga region that burned two or even three times (3% of the disturbed areas) during the investigated period, primarily in plantation forests dominated by Scots pine [72].

The importance of climatic factors in estimating forest recovery on the BAs using remote sensing data has been recognised in various regions worldwide [29,38,47,68]. Some studies suggest that a dry weather not only increases wildfire risk, but also delays or even lead to recruitment failure in post-fire recovery of boreal forests in southern Siberia [28,42,68]. Based on the results from the multiple linear regression analysis significant at the 95% level (P-value < 0.05), our study shows that climate parameters (LST and Pr) are responsible for variations in the forest recovery at different BS sites after

 doi:10.20944/preprints202409.1781.v

the wildfires. While the best regression equation included both climatic factors averaged over the estimated period (May to September), the statistics indicate that temperature (LST) had a stronger impact on the forest recovery (vegetation growth) compared to precipitation. The strongest relationship of the forest recovery with the climate factors was shown in the moderate BS area. Considering the IPCC (Intergovernmental Panel on Climate Change) scenarios in the context of a changing climate worldwide, which forecasts increasing LST during the coming decades [95], it becomes clear that such factors play a crucial role in the long-term recovery patterns of post-fire ecosystems.

Our results contribute to a better understanding of the integral assessment between BS, time-series spectral NBR metrics, climate factors, and forest spatio-temporal recovery after large wildfires in the Middle Volga region during the 2000-2023 period. The results of the current study are consistent with field-based validation plots established across the investigated area. This research can help forest managers predict the post-fire forest recovery capacity of broadleaved and mixed coniferous stands based on the observed burn severity regimes, using scientific and rational arrangements. Priority should be given to regions prone to widespread forest fires, such as the Republic Mari El and Nizhegorodskaya oblast, when implementing strategies aimed at restoring the pre-fire status of forest ecosystems. The generated maps, regression models, and trend analysis of forest recovery at a spatial resolution relevant to forest management can be valuable tools for local authorities and decision makers in strategic planning.

Future studies are needed to enhance and expand the scope the analyses carried out in this research. We encourage conducting studies analysing recovery patterns of different tree species and forest types using multispectral imagery to help in modelling the composition of post-fire ecosystems. More efforts are required to explore long-term competitive relationships and forest recovery processes using sensors with high spatial and temporal resolution (e.g., SENTINEL, Resurs-P, Canopus-B), and supplementing with field survey data. In addition to climatic factors, forest recovery can also be influenced by various other driving factors, including topography, soil moisture, competitive interactions, and socio-economic data specific to each satellite image. Finally, more sensitive spectral vegetation indices, IPCC climate change scenarios for forest management and recent time-series models (eg. Long short-term memory) are also required in future research.

5. Conclusions

In this study, we used Landsat time series data to examine spectral forest recovery rates and associated drivers on burned area of the Middle Volga region of the Russian Federation over the past 20 years. For the first time in this region, we provide spatio-temporally explicit, multi-decadal trends in forest recovery, revealing a shift from coniferous to broadleaved species dominance. This research suggests a cost-effective methodology using large-scale spatiotemporal remote sensing data and deep learning algorithms to estimate the recovery of wildfire-affected forests. Post-fire trends and rates of forest recovery were assessed using the LandTrendr algorithm in the Google Earth Engine platform. Our results indicated that the forest recovery trajectories were highly variable and dependent on the burn severity of the affected areas. The use of several metrics measuring spectral forest recovery rates allowed us to gain valuable insights into the characteristics and patterns of forest recovery at the regional scale. The results clearly showed an increasing forest recovery trend, both spatially and temporally, across the Middle Volga region, with the highest recovery rate found in the high and moderate BS classes. Consistent with other studies [28–31], we confirmed that forest recovery has a good coupling relationship with climatic factors, especially land surface temperature. The results are applicable to other BAs and may help researchers more effectively use the GEE platforms and time series images to map forest recovery, recovery rates and their trends for further environmental studies. Furthermore, the findings can help management decisions by providing cost-effective strategies under changing climatic conditions, including carbon forecasting in forest ecosystems, vegetation regeneration, and climate-smart forestry.

Author Contributions: Conceptualization, E.K., A.Y., O.V., J.S., and J.W.; methodology, E.K., L.T., A.Y., O.V., J.S., and J.W.; software, L.T., S.G., S.L., D.D., An.Y.; validation, E.K., L.T., O.V., S.L., D.D. and An.Y.; formal

 doi:10.20944/preprints202409.1781.v

analysis, E.K., L.T., A.Y., J.W., and S.L; investigation, L.T., O.V., S.L., D.D., and An.Y.; resources, L.T., S.L, D.D., and An.Y.; data curation, L.T., S.G., S.L., D.D., and An.Y.; writing—original draft preparation, E.K., A.Y., O.V.; writing—review and editing, E.K., A.Y., J.S., O.V., and J.W.; visualization, S.L, S.D., D.D., and An.Y.; supervision, E.K.; project administration, E.K., A.Y., J.S., and J.W; funding acquisition, E.K., A.Y., S.G. All authors have read and agreed to the published version of the manuscript.

Funding: The reported study was funded in the framework of Russian Science Foundation grant No. 22-16-00094, https://rscf.ru/project/22-16-00094/ (accessed on 16 September 2024).

Data Availability Statement: Statement: The data presented in this study is available in the article. More information is available on request from the corresponding authors.

Acknowledgments: The authors are grateful to the anonymous reviewers for their valuable feedback and guidance in improving the initial version of this manuscript in multiple ways.

Conflicts of Interest: The authors declare no conflict of interest. The funders had no role in the design of the study; in the collection, analyses, or interpretation of data; in the writing of the manuscript; or in the decision to publish the results.

References

1. Poorter, L.; Craven, D.; Jakovac, C.C.; van der Sande, M.T.; Amissah, L.; Bongers, F.; Chazdon, R.L.; Farrior, C.E.; Kambach, S.; Meave, J.A.; et al. Multidimensional tropical forest recovery. *Science* **2021**, *374*, 1370-1376. [CrossRef]
2. Alayan, R.; Rotich, B.; Lakner, Z.A. Comprehensive framework for forest restoration after forest fires in theory and practice: a systematic review. *Forests* **2022**, *13*, 1354. [CrossRef]
3. Strassburg, B.B.N.; Beyer, H.L.; Crouzeilles, R.; Iribarrem, A.; Barros, F.; de Siqueira, M.F.; Sánchez-Tapia, A.; Balmford, A.; Sansevero, J.B.B.; Brancalion, P.H.S.; et al. Strategic approaches to restoring ecosystems can triple conservation gains and halve costs. *Nat Ecol Evol*. **2019**, *3*, 62-70. [CrossRef]
4. FAO. Global Forest Resources Assessment 2020: Main Report; FAO: Rome, Italy, 2020. 184 p. [CrossRef]
5. Chen, X.; Chen, W.; Xu, M. Remote-sensing monitoring of postfire vegetation dynamics in the Greater Hinggan mountain range based on long time-series data: analysis of the effects of six topographic and climatic factors. *Remote Sens*. **2022**, *14*, 2958. [CrossRef]
6. Lasslop, G.; Hantson, S.; Harrison, S.P.; Bachelet, D.; Burton, C.; Forkel, M.; Forrest, M.; Li, F.; Melton, J.R.; Yue, C.; et al. Global ecosystems and fire: Multi-model assessment of fire-induced tree-cover and carbon storage reduction. *Glob. Chang. Biol*. **2020**, *26*, 5027–5041. [CrossRef]
7. Vasques, A.; Baudena, M.; Vallejo, V.R.; Kefi, S.; Bautista, S.; Santana, V.M.; Baeza, M.J.; Maia, P.; Keizer, J.J.; Rietkerk, M. Post-fire regeneration traits of understorey shrub species modulate successional responses to high severity fire in Mediterranean pine forests. *Ecosystems* **2022**, 26, 146-160. [CrossRef]
8. Otoda, T.; Doi, T.; Sakamoto, K.; Hirobe, M.; Nachin, B.; Yoshikawa, K. Frequent fires may alter the future composition of the boreal forest in northern Mongolia. *J. For. Res*. **2012**, *18*, 246–255. [CrossRef]
9. Chu, T.; Guo, X. Remote sensing techniques in monitoring post-fire effects and patterns of forest recovery in boreal forest regions: a review. *Remote Sens*. **2014**, *6*, 470-520. [CrossRef]
10. Kurbanov, E.; Vorobev, O.; Lezhnin, S.; Sha, J.; Wang, J.; Li, X.; Cole, J.; Dergunov, D.; Wang, Y. Remote sensing of forest burnt area, burn severity, and post-fire recovery: a review. *Remote Sens.* **2022**, *14*, 4714. [CrossRef]
11. Souza-Alonso, P.; Saiz, G.; García, R.A.; Pauchard, A.; Ferreira, A.; Merino, A. Post-fire ecological restoration in Latin American forest ecosystems: insights and lessons from the last two decades. *For. Ecol. Manag*. **2022**, *509*, 120083. [CrossRef]
12. Frazier, R. J.; Coops, N. C.; Wulder, M. A.; Hermosilla, T.; White, J. C. Analyzing spatial and temporal variability in short-term rates of post-fire vegetation return from Landsat time series. *Remote Sens. Environ*. **2018**, *205*. 32-45. [CrossRef]
13. Gitas, I.; Mitri, G.; Veraverbeke, S.; Polychronaki, A. Advances in remote sensing of post-fire vegetation recovery monitoring—a review. In *Remote Sensing of Biomass—Principles and Applications*; Fatoyinbo, L., Ed.; InTech: London, UK, 2012; ISBN 978-953-51-0313-4.
14. Perez-Cabello, F.; Montorio, R.; Alves, D.B. Remote sensing techniques to assess post-fire vegetation recovery. *Current Opinion in Environmental Science & Health* **2021**, *21*, 100251. [CrossRef]
15. Alatorre, L.; Sánchez, E.; Amado, J.; Wiebe, L.; Torres, M.; Rojas, H.; Bravo, L.; López, E. Analysis of the temporal and spatial evolution of recovery and degradation processes in vegetated areas using a time series of Landsat TM images (1986-2011): central region of Chihuahua, Mexico. *Open J. For.* **2015**, *5*, 162-180. [CrossRef]
16. Bartels, S.F.; Chen H.Y.H.; Wulder, M.A.; White, J.C. Trends in post-disturbance recovery rates of Canada's forests following wildfire and harvest. *For Ecol Manag.* **2016**, *361*:194–207. [CrossRef]

17. Hislop, S.; Haywood, A.; Jones, S.; Soto-Berelov, M.; Skidmore, A.; Nguyen, T.H. A satellite data driven approach to monitoring and reporting fire disturbance and recovery across boreal and temperate forests. *Int. J. Appl. Earth Obs. Geoinf*. **2020**, *87*, 102034. [CrossRef]
18. Chu, T.; Guo, X.; Takeda, K. Effects of burn severity and environmental conditions on post-fire regeneration in Siberian Larch forest. *Forests* **2017**, *8*, 76. [CrossRef]
19. Santana, N.C.; Júnior, O.A.d.C.; Gomes, R.A.T.; Fontes Guimarães, R. Comparison of post-fire patterns in Brazilian savanna and tropical forest from remote sensing time series. *ISPRS Int. J. Geo-Inf.* **2020**, *9*, 659. [CrossRef]
20. Ryu, J.-H.; Han, K.-S.; Hong, S.; Park, N.-W.; Lee, Y.-W.; Cho, J. Satellite-based evaluation of the post-fire recovery process from the worst forest fire case in South Korea. *Remote Sens.* **2018**, *10*, 918. [CrossRef]
21. Avetisyan, D.; Velizarova, E.; Filchev, L. Post-fire forest vegetation state monitoring through satellite remote sensing and in situ data. *Remote Sens.* **2022**, *14*, 6266. [CrossRef]
22. Ba, R.; Lovallo, M.; Song, W.; Zhang, H.; Telesca, L. Multifractal analysis of MODIS Aqua and Terra satellite time series of normalized difference vegetation index and enhanced vegetation index of sites affected by wildfires. *Entropy* **2022**, *24*, 1748. [CrossRef]
23. Bonannella, C.; Chirici, G.; Travaglini, D.; Pecchi, M.; Vangi, E.; D'Amico, G.; Giannetti, F. Characterization of wildfires and harvesting forest disturbances and recovery using Landsat time series: a case study in Mediterranean forests in central Italy. *Fire* **2022**, *5*, 68. [CrossRef]
24. Vandansambuu, B.; Gantumur, B.; Wu, F.; Byambasuren, O.; Bayarsaikhan, S.; Chantsal, N.; Batsaikhan, N.; Bao, Y.; Vandansambuu, B.; Jimseekhuu, M.-E. Assessment of burn severity and monitoring of the wildfire recovery process in Mongolia. *Fire* **2023**, *6*, 373. [CrossRef]
25. White, J.C.; Hermosilla, T.; Wulder, M.A.; Coops, N.C. Mapping, validating, and interpreting spatio-temporal trends in post-disturbance forest recovery. *Remote Sens. Environ*. **2022,** *271*, 112904. [CrossRef]
26. Meneses, B.M. Vegetation recovery patterns in burned areas assessed with Landsat 8 OLI imagery and environmental biophysical data. *Fire* **2021**, *4*, 76. [CrossRef]
27. Han, A.; Qing, S.; Bao, Y.; Na, L.; Bao, Y.; Liu, X.; Zhang, J.; Wang, C. Short-term effects of fire severity on vegetation based on sentinel-2 satellite data. *Sustainability* **2021**, *13*, 432. [CrossRef]
28. Sun, Q.; Burrell, A.; Barrett, K.; Kukavskaya, E.; Buryak, L.; Kaduk, J.; Baxter, R. Climate variability may delay post-fire recovery of boreal forest in southern Siberia, Russia. *Remote Sens*. **2021**, *13*, 2247. [CrossRef]
29. Hao, B.; Xu, X.; Wu, F.; Tan, L. Long-term effects of fire severity and climatic factors on post-forest-fire vegetation recovery. *Forests* **2022**, *13*, 883. [CrossRef]
30. Wilson, A.M.; Latimer, A.M.; Silander, J.A. Climatic controls on ecosystem resilience: postfire regeneration in the Cape floristic region of South Africa. *Proc. Natl. Acad. Sci*. USA **2015**, *112*, 9058–9063. [CrossRef] [PubMed]
31. Viana-Soto, A.; Aguado, I.; Salas, J.; García, M. Identifying post-fire recovery trajectories and driving factors using Landsat Time series in fire-prone Mediterranean pine forests. *Remote Sens.* **2020**, *12*, 1499. [CrossRef]
32. Bassett, M.; Leonard, S.W.; Chia, E.K.; Clarke, M.F.; Bennett, A.F. Interacting effects of fire severity, time since fire and topography on vegetation structure after wildfire. *For. Ecol. Manag*. **2017**, *396*, 26–34. [CrossRef]
33. Haffey, C.; Sisk, T.D.; Allen, C.D.; Thode, A.E.; Margolis, E.Q. Limits to ponderosa pine regeneration following large high-severity forest fires in the United States Southwest. *Fire Ecol*. **2018**, *14*, 143–163. [CrossRef]
34. Rammer, W.; Braziunas, K.H.; Hansen, W.D.; Ratajczak, Z.; Westerling, A.L.; Turner, M. G.; Seidl, R. Widespread regeneration failure in forests of Greater Yellowstone under scenarios of future climate and fire. *Glob. Chang Biol*. **2021**, *27*, 4339–4351. [CrossRef]
35. He, Z.; Wang, L.; Luo, J.; Zhang, B.; Deng, Q.; Liu, H. Topographic factors drive short-term understory revegetation in burned areas. *Fire* **2022**, *5*, 171. [CrossRef]
36. Christopoulou, A.; Mallinis, G.; Vassilakis, E.; Farangitakis, G.-P.; Fyllas, N.M.; Kokkoris, G.D.; Arianoutsou, M. Assessing the impact of different landscape features on post-fire forest recovery with multitemporal remote sensing data: The case of Mount Taygetos (southern Greece). *Int. J. Wildl. Fire,* **2019**, *28*, 521–532. [CrossRef]
37. Alegria, C. Vegetation monitoring and post-fire recovery: a case study in the centre inland of Portugal. *Sustainability* **2022**, *14*, 12698. [CrossRef]
38. Blanco-Rodríguez, M.Á.; Ameztegui, A.; Gelabert, P.; Rodrigues, M.; Coll, L. Short-term recovery of post-fire vegetation is primarily limited by drought in Mediterranean forest ecosystems. *Fire Ecol.* **2023**, *19*, 68. [CrossRef]
39. Maillard, O. Post-Fire Natural Regeneration Trends in Bolivia: 2001–2021. *Fire* **2023**, *6*, 18. [CrossRef]
40. Key, C.H.; Benson, N.C. Landscape assessment: Remote sensing of severity, the normalized burn ratio. *In FIREMON: Fire effects monitoring and inventory system*; USDA Forest Service, Rocky Mountain Research Station, Fort Collins: Denver, CO, USA, 2006; pp. 305–325.

41. Collins, B.M.; Roller, G.B. Early forest dynamics in stand-replacing fire patches in the northern Sierra Nevada. *Landscape Ecol*. **2013**, *28*, 1801–1813. [CrossRef]
42. Barrett, K.; Baxter, R.; Kukavskaya, E.; Balzter, H.; Shvetsov, E.; Buryak, L. Postfire recruitment failure in Scots pine forests of southern Siberia. *Remote Sens. Environ*. **2020**, *237*, 111539. [CrossRef]
43. Guz, J.; Sangermano, F.; Kulakowski, D. The Influence of burn severity on post-fire spectral recovery of three fires in the southern Rocky Mountains. *Remote Sens.* **2022**, *14*, 1363. [CrossRef]
44. Dvornikov, Y.; Novenko, E.; Korets, M.; Olchev, A. Wildfire dynamics along a north-central Siberian latitudinal transect assessed using Landsat imagery. *Remote Sens.* **2022**, *14*, 790. [CrossRef]
45. Crotteau, J.S.; Morgan Varner, J.; Ritchie, M.W. Post-fire regeneration across a fire severity gradient in the southern Cascades. *For. Ecol. Manage*. **2013**, *287*, 103–112. [CrossRef]
46. Viana-Soto, A.; Okujeni, A.; Pflugmacher, D.; García, M.; Aguado, I.; Hostert, P. Quantifying post-fire shifts in woody-vegetation cover composition in Mediterranean pine forests using Landsat time series and regression-based unmixing. *Remote Sens. Environ*. **2022,** *281*, 113239. [CrossRef]
47. Williams, N.G.; Lucash, M.S.; Ouellette, M.R.; Brussel, T.; Gustafson, E. J.; Weiss, S. A.; Sturtevant, B. R.; Schepaschenko, D. G.; Shvidenko, A. Z. Simulating dynamic fire regime and vegetation change in a warming Siberia. *Fire ecol.* **2023**, *19*, 33. [CrossRef]
48. Wan, H.Y.; Olson, A.C.; Muncey, K.D.; St Clair, S.B. Legacy effects of fire size and severity on forest regeneration, recruitment, and wildlife activity in aspen forests. *For. Ecol. Manag*. **2014**, *329*, 59–68. [CrossRef]
49. Lewis J.S.; St. Clair, S.B.; Fairweather, M.L.; Rubin, E.S. Fire severity and ungulate herbivory shape forest regeneration and recruitment after a large mixed-severity wildfire. *For. Ecol. Manag*. **2024**, *555*, 121692. [CrossRef]
50. Gorelick, N.; Hancher, M.; Dixon, M.; Ilyushchenko, S.; Thau, D.; Moore, R. Google Earth Engine: Planetary-scale geospatial analysis for everyone. *Remote Sens. Environ*. **2017**, *202*, 18–27. [CrossRef]
51. Tamiminia, H.; Salehi, B.; Mahdianpari, M.; Quackenbush, L.; Adeli, S.; Brisco, B. Google Earth Engine for geo-big data applications: A meta-analysis and systematic review. *ISPRS J. Photogramm. Remote Sens*. **2020**, *164*, 152–170. [CrossRef]
52. Velastegui-Montoya, A.; Montalván-Burbano, N.; Carrión-Mero, P.; Rivera-Torres, H.; Sadeck, L.; Adami, M. Google Earth Engine: a global analysis and future trends. *Remote Sens.* **2023**, *15*, 3675. [CrossRef]
53. Huang, C.; Goward, S.N.; Masek, J.G.; Thomas, N.; Zhu, Z.; Vogelmann, J.E. An automated approach for reconstructing recent forest disturbance history using dense Landsat time series stacks. *Remote Sens. Environ.* **2010**, *114*, 183–198. [CrossRef]
54. Jamali, S.; Jönsson, P.; Eklundh, L.; Ardö, J.; Seaquist, J. Detecting changes in vegetation trends using time series segmentation. *Remote Sens. Environ.* **2015**, *156*, 182–195. [CrossRef]
55. Zhu, Z. Change detection using Landsat time series: A review of frequencies, preprocessing, algorithms, and applications. *ISPRS J. Photogramm. Remote Sens*. **2017**, *130*, 370–384. [CrossRef]
56. Kennedy, R.E.; Yang Z.; Cohen, W.B. Detecting trends in forest disturbance and recovery using yearly Landsat time series: 1. LandTrendr—temporal segmentation algorithms. *Remote Sens. Env.* **2010,** *114*, 2897–2910. [CrossRef]
57. Kennedy, R.E.; Yang, Z.; Gorelick, N.; Braaten, J.; Cavalcante, L.; Cohen, W.B.; Healey, S. Implementation of the LandTrendr algorithm on Google Earth Engine. *Remote Sens*. **2018**, *10*, 691. [CrossRef]
58. Cohen, W.; Yang, Z.; Healey, S.; Kennedy, R.; Gorelick, N. A LandTrendr multispectral ensemble for forest disturbance detection. *Remote Sens. Env*. **2018**, *205*, 131–140. [CrossRef]
59. Cohen, W.B.; Healey, S.P.; Yang, Z.; Stehman, S.V.; Brewer, C.K.; Brooks, E.B.; Gorelick, N.; Huang, C.; Hughes, M.J.; Kennedy, R.E.; et al. How similar are forest disturbance maps derived from different Landsat time series algorithms? *Forests* **2017**, *8*, 98. [CrossRef]
60. Bonney, M.T.; He, Y.; Myint, S.W. Contextualizing the 2019–2020 Kangaroo island bushfires: quantifying landscape-level influences on past severity and recovery with Landsat and Google Earth Engine. *Remote Sens.* **2020**, *12*, 3942. [CrossRef]
61. Han, Y.; Ke, Y.; Zhu, L.; Feng, H.; Zhang, Q.; Sun, Z.; Zhu, L. Tracking vegetation degradation and recovery in multiple mining areas in Beijing, China, based on time-series Landsat imagery. *GISci. Remote Sens*. **2021**, *58*, 1477-1496. [CrossRef]
62. Hird, J.N.; Kariyeva, J.; McDermid, G.J. Satellite time series and Google Earth Engine democratize the process of forest-recovery monitoring over large areas. *Remote Sens.* **2021**, *13*, 4745. [CrossRef]
63. Zhang, Q.; Homayouni, S.; Zhao, P.; Zhou M. Burned vegetation recovery trajectory and its driving factors using satellite remote-sensing datasets in the Great Xing'An forest region of Inner Mongolia. *Int. J. Wildland Fire* **2023**, *32*, 244-261. [CrossRef]
64. Bright, B.C.; Hudak, A.T.; Kennedy, R.E.; Braaten, J.D.; Khalyani, A.H. Examining post-fire vegetation recovery with Landsat time series analysis in three western North American forest types. *Fire ecol.* **2019**, *15*, 8. [CrossRef]

65. Hua, J.; Chen, G.; Yu, L.; Ye, Q.; Jiao, H.; Luo, X. Improved mapping of long-term forest disturbance and recovery dynamics in the subtropical China using all available Landsat time-series imagery on Google Earth Engine platform. *IEEE J. Sel. Top. Appl. Earth Obs. Remote Sens*. **2021**, *14*, 2754-2768. [CrossRef]
66. Ren, H.; Ren, C.; Wang, Z.; Jia, M.; Yu, W.; Liu, P.; Xia, C. Continuous tracking of forest disturbance and recovery in the Greater Khingan mountains from annual Landsat Imagery. *Remote Sens.* **2023**, *15*, 5426. [CrossRef]
67. Hambinintsoa, A.H.R.; Harto, A.B.; Virtriana, R. Spatio-temporal spectral trajectory pattern to continuous maps of forest disturbance and recovery: case of tropical forests of Vatovavy Fitovinany, Madagascar. *Model. Earth Syst. Environ.* **2023**, *9*, 3597–3608. [CrossRef]
68. Burrell, A.; Kukavskaya, E.; Baxter, R.; Sun, Q.; Barrett, K. Post-fire recruitment failure as a driver of forest to non-forest ecosystem shifts in boreal regions. *In book* "Ecosystem Collapse and Climate Change"; Eds. Canadell, J.G.; Jackson, R.B., Springer: Cham, Switzerland, 2021, Vol. 241, pp. 69-100. [CrossRef]
69. Shvetsov, E.G.; Kukavskaya, E.A.; Buryak, L.V.; Barrett, K. Assessment of post-fire vegetation recovery in Southern Siberia using remote sensing observations. Environ. Res. Lett. **2019**, *14*, 05500. [CrossRef]
70. Vorobyov, O.N.; Kurbanov, E.A.; Lezhnin, S.A.; Gubayev, A.V.; Dergunov, D.M.; Tarasova, L.V. Spatio-temporal analysis of forest cover in the Middle Volga using landscape indices and Landsat satellite data. *Current problems in remote sensing of the Earth from space* **2023**, *20*, 144-159. (In Russian) [CrossRef]
71. Perevedentsev, Y.; Sherstyukov, B.; Gusarov, A.; Aukhadeev, T.; Mirsaeva, N. Climate-induced fire hazard in forests in the Volga federal district of European Russia during 1992–2020. *Climate* **2022**, 10, 110. [CrossRef]
72. Kurbanov, E.; Vorobev, O.; Lezhnin, S.; Dergunov, D.; Wang, J.; Sha, J.; Gubaev, A.; Tarasova, L.; Wang, Y. Temporal and spatial analyses of forest burnt area in the Middle Volga region based on satellite imagery and climatic Factors. *Climate* **2024**, *12*, 45. [CrossRef]
73. Loboda, T; Krankina, O.; Savin, I.; Kurbanov, E.; Joanne, H. Land Management and the impact of the 2010 extreme drought event on the agricultural and ecological systems of European Russia. *In Book* "Land-Cover and Land-Use Changes in Eastern Europe after the Collapse of the Soviet Union in 1991"; Eds. Gutman, G.; Volker, R., Springer International Publishing. Switzerland AG, 2017, pp. 173–192. [CrossRef]
74. Vorobiev, O.N.; Kurbanov, E.A. Remote monitoring of vegetation regeneration dynamics on burnt areas of Mari Zavolzhje forests. *Current problems in remote sensing of the Earth from space* **2017**, *14*, 84-97 (In Russian) [CrossRef]
75. Kurbanov, E.A.; Post W.M. Changes in area and carbon in forests of the Middle Zavolgie: a regional case study of Russian forests. *Climatic Change* **2002**, *55*, 157–171. [CrossRef]
76. Kurbanov, E. Carbon in pine forest ecosystems of Middle Zavolgie, Russia. *Technical Report 2*. European Forest Institute, Finland, 2000. [CrossRef]
77. Lerink, B.; Hassegawa, M.; Kryshen, A.; Kovalev, A.; Kurbanov, E.; Nabuurs, G.J., Moshnikov, S.; Verkerk, P.J. Climate-smart forestry in Russia and potential climate change mitigation benefits. In Book *Russian Forests and Climate Change. What Science Can Tell Us 11*. Leskinen, P., Lindner, M., Verkerk, P.J., Nabuurs G.J., Van Brusselen, J., Kulikova, E., Hassegawa, M., Lerink, B. Eds.; European Forest Institute, Finland, 2020, pp. 73–103. [CrossRef]
78. Vorobyov, O.N.; Lezhnin, S.A.; Kurbanov, E.A.; Yahyayev, A.B.; Dergunov, D.M.; Tarasova, L.V., Yastrebova, A.V. Predictive analysis of forest cover in the Middle Volga Region based on time series and climate scenarios. *Current problems in remote sensing of the Earth from space* **2024**, *21*, 115-130. (In Russian) [CrossRef]
79. Foga, S.; Scaramuzza, P.L.; Guo, S.; Zhu, Z.; Dilley, R.D.; Beckmann, T.; Schmidt, G.L.; Dwyer, J.L.; Joseph Hughes, M.; Laue, B. Cloud detection algorithm comparison and validation for operational Landsat data products. *Remote Sens. Environ.* **2017**, *194*, 379–390. [CrossRef]
80. Vermote, E.; Justice, C.; Claverie, M.; Franch, B. Preliminary analysis of the performance of the Landsat 8/OLI land surface reflectance product. *Remote Sens. Environ*. **2016**, *185*, 46–56. [CrossRef]
81. Claverie, M.; Vermote, E.F.; Franch, B.; Masek, J.G. Evaluation of the Landsat-5 TM and Landsat-7 ETM+ Surface Reflectance Products. *Remote Sens. Environ.* **2015**, *169*, 390–403. [**CrossRef**]
82. Roy, D.P.; Kovalskyy, V.; Zhang, H.K.; Vermote, E.F.; Yan, L.; Kumar, S.S.; Egorov, A. Characterization of Landsat-7 to Landsat-8 reflective wavelength and normalized difference vegetation index continuity. *Remote Sens. Environ*. **2016**, *185*, 57–70. [CrossRef]
83. Kurbanov, E.; Vorobyev, O.; Leznin, S.; Polevshikova, Y.; Demisheva, E. Assessment of burn severity in Middle Povozhje with Landsat multitemporal data. *Int. J. Wildland Fire* **2017**, *26*, 772–782. [CrossRef]
84. Flood, N. Seasonal composite Landsat TM/ETM+ images using the Medoid (A multi-dimensional median). *Remote Sens*. **2013**, *5*, 6481–6500. [CrossRef]
85. Mann, H.B. Nonparametric tests against trend. *Econometrica* **1945,** *13*, 245–259. [CrossRef]
86. Kendall, M.G. *Rank correlation methods*. Charles Griffin, Oxford, England, 1955.
87. Sen, P.K. Estimates of the regression coefficient based on Kendall's tau. *J. Am. Stat. Assoc*. **1968**, *63*, 1379–1389. [CrossRef]

88. Theil, H. A rank-invariant method of linear and polynomial regression analysis. In: *Henri Theil's contributions to economics and econometrics*. Springer, 1992, pp. 345–381. [CrossRef]
89. Gocic, M.; Trajkovic, S. Analysis of changes in meteorological variables using Mann-Kendall and Sen's slope estimator statistical tests in Serbia. *Global and Planetary Change*. **2013**, *100*, 172–182. [CrossRef]
90. Yuan, J.; Bian, Z.; Yan, Q.; Gu, Z.; Yu, H. An approach to the temporal and spatial characteristics of vegetation in the growing season in Western China. *Remote Sens*. **2020**, *12*, 945. [CrossRef]
91. Kennedy, R.E.; Yang Z.; Cohen, W.B.; Pfaff, E.; Braaten, J.; Nelson, P. Spatial and temporal patterns of forest disturbance and regrowth within the area of the Northwest Forest Plan. *Remote Sens. Env.* **2012,** *122*, 117–133. [CrossRef]
92. Pickell, P.D.; Hermosilla, T.; Frazier, R.J.; Coops, N.C.; Wulder, M.A. Forest recovery trends derived from Landsat time series for North American boreal forests. *Int. J. Remote Sens*. **2016**, *37*, 138-149, [CrossRef]
93. White, J.C.; Saarinen, N.; Wulder, M.A.; Kankare, V.; Hermosilla, T.; Coops, N.C.; Holopainen, M.; Hyyppä, J.; Vastaranta, M. Assessing spectral measures of post-harvest forest recovery with field plot data. *Int. J. Appl. Earth Obs. Geoinf*. **2019**, *80*, 102–114. [CrossRef]
94. Hansen, M. C.; Potapov, P. V.; Moore, R.; Hancher, M.; Turubanova, S. A.; Tyukavina, A.; Thau, D.; Stehman, S. V.; Goetz, S. J.; Loveland, T. R.; Kommareddy, A.; Egorov, A.; Chini, L.; Justice, C. O.; Townshend, J. R. G. High-resolution global maps of 21st-century forest cover change. *Science*. **2013**, *342*, 850-853. https://doi.org/10.1126/science.1244693
95. IPCC. Climate Change 2013: The Physical Science Basis. Contribution of Working Group I to the Fifth Assessment Report of the Intergovernmental Panel on Climate Change, [Stocker, T.F., D. Qin, G.-K. Plattner, et. al. (eds.)], Cambridge University Press, Cambridge, UK and NY, NY, USA, 2013, 1535 pp. [CrossRef]